Monthly Notices
of the
ROYAL ASTRONOMICAL SOCIETY

Mon. Not. R. Astron. Soc. **416,** 1566–1584 (2011) doi:10.1111/j.1365-2966.2011.19160.x

On the impact of empirical and theoretical star formation laws on galaxy formation

Claudia del P. Lagos,[1]★ Cedric G. Lacey,[1] Carlton M. Baugh,[1] Richard G. Bower[1] and Andrew J. Benson[2]

[1]*Institute for Computational Cosmology, Department of Physics, University of Durham, South Road, Durham DH1 3LE*
[2]*California Institute of Technology, Pasadena, CA 91125, USA*

Accepted 2011 May 28. Received 2011 May 18; in original form 2010 November 24

ABSTRACT

We investigate the consequences of applying different star formation laws in the galaxy formation model GALFORM. Three broad star formation laws are implemented: the empirical relations of Kennicutt and Schmidt and Blitz & Rosolowsky and the theoretical model of Krumholz, McKee & Tumlinson. These laws have no free parameters once calibrated against observations of the star formation rate (SFR) and gas surface density in nearby galaxies. We start from published models, and investigate which observables are sensitive to a change in the star formation law, without altering any other model parameters. We show that changing the star formation law (i) does not significantly affect either the star formation history of the universe or the galaxy luminosity functions in the optical and near-infrared, due to an effective balance between the quiescent and burst star formation modes, (ii) greatly affects the cold gas contents of galaxies and (iii) changes the location of galaxies in the SFR versus stellar mass plane, so that a second sequence of 'passive' galaxies arises, in addition to the known 'active' sequence. We show that this plane can be used to discriminate between the star formation laws.

Key words: stars: formation – galaxies: evolution – galaxies: formation – galaxies: ISM.

1 INTRODUCTION

A proper understanding of how galaxies form and evolve must include a description of star formation (SF) and the physics that regulate this phenomenon. The lack of a theoretical description of SF has forced galaxy formation modellers to adopt simple parametric recipes (e.g. White & Frenk 1991; Lacey et al. 1993; Cole et al. 1994, 2000; Kauffmann & Charlot 1998; Springel et al. 2001; Cora 2006; Monaco, Fontanot & Taffoni 2007; Cattaneo et al. 2008; Lagos, Cora & Padilla 2008).

Two forms commonly adopted for the SF law relate the SF rate (SFR) per unit area, $\Sigma_{\rm SFR}$, to the gas surface density either as (i) $\Sigma_{\rm SFR} \propto \Sigma_{\rm gas}^{N}$ (Schmidt 1959) or (ii) $\Sigma_{\rm SFR} \propto \Sigma_{\rm gas}/\tau_{\rm dyn}$ (Shu 1973), where $\tau_{\rm dyn}$ is a dynamical time-scale. Observational constraints on the form of the SF law remained scarce for many years. Early observations of individual galaxies gave conflicting results for the power-law index N in relation (i) above, returning values over the range $N \approx 1$–3 (see Sanduleak 1969 and Hartwick 1971 for extreme examples). Nor was it clear, when applying form (ii), whether a local or global dynamical time-scale $\tau_{\rm dyn}$ is more relevant [e.g. the local free-fall time of the gas or the orbital time around a galaxy; see Madore (1977) and Solomon & Sage (1988), respectively]. The situation improved with the observational sample constructed by Kennicutt (1998, hereafter K98), which he used to examine correlations between the global SFR and gas surface densities for a wide range of nearby galaxies, from normal spirals to starbursts (SBs). K98 found that the global relation was remarkably well fitted by (i), with $N = 1.40 \pm 0.15$, but also nearly equally well fitted by (ii), when taking $\tau_{\rm dyn}$ equal to the disc orbital time. However, observational studies of the resolved radial profiles of SFR and gas in individual galaxies showed a breakdown of the power-law relation at low gas surface densities, with a sharp cut-off in $\Sigma_{\rm SFR}$ below a critical gas surface density (Kennicutt 1989; Martin & Kennicutt 2001). This feature was interpreted using simple gravitational arguments as marking the onset of dynamical stability in the gas layer, thereby allowing the fragmentation of the gas into star-forming clouds at gas surface densities above a threshold value (Toomre 1964).

Over the past 10 years, enormous advances in the characterization of the SF law have been made possible through the availability of new, high-quality, spatially resolved observations of H I (e.g. Walter et al. 2008) and CO (e.g. Helfer et al. 2003; Leroy et al. 2009), and of ultraviolet (UV) and infrared (IR) SFR tracers in samples of nearby galaxies. These data have allowed the accurate estimation of the molecular and atomic hydrogen content of galaxies over a wide range of morphologies and gas fractions. In addition, more reliable

★E-mail: c.d.p.lagos@durham.ac.uk

estimates of unobscured SF in the UV (e.g. Gil de Paz et al. 2007) and of dust-obscured SF in the IR (e.g. Calzetti et al. 2007) have allowed better determinations of the SFR, both globally and within individual SF regions. There is now support for a correlation between $\Sigma_{\rm SFR}$ and the molecular gas surface density, $\Sigma_{\rm mol}$, of the form $\Sigma_{\rm SFR} \propto \Sigma_{\rm mol}$ (Wong & Blitz 2002; Kennicutt et al. 2007; Bigiel et al. 2008). This relation is much stronger than that with either the total cold gas or atomic hydrogen surface densities. At high redshifts, there are indications that the same form, $\Sigma_{\rm SFR} \propto \Sigma_{\rm mol}$, could hold (Bouché et al. 2007; Genzel et al. 2010). The correlation of $\Sigma_{\rm SFR}$ with $\Sigma_{\rm mol}$ seems physically reasonable since stars are observed to form in dense molecular gas clouds (see Solomon & Vanden Bout 2005, for a review).

The threshold in the SF law suggested by the observations of Kennicutt (1989) and Martin & Kennicutt (2001) has since been studied in more detail. SF activity has been observed in galaxies even at low gas surface densities ($\Sigma_{\rm gas} \leq 10\,{\rm M}_\odot\,{\rm pc}^{-2}$; Heyer et al. 2004; Bigiel et al. 2008; Fumagalli & Gavazzi 2008; Roychowdhury et al. 2009; Wyder et al. 2009), but following a steeper relation in $\Sigma_{\rm gas}$ compared to the SF law found at higher gas surface densities, suggesting a different regime of SF activity. Furthermore, Blitz & Rosolowsky (2006, hereafter BR06) and Leroy et al. (2008) found that the ratio of molecular-to-atomic hydrogen surface densities, $R_{\rm mol}$, is well fitted by a power-law function of the hydrostatic pressure in galactic discs, $R_{\rm mol} \propto P_{\rm ext}^{\alpha}$, with the same relation holding from dwarf to normal spiral galaxies. An empirical SF law emerges from these studies in which the relationship between $R_{\rm mol}$ and $P_{\rm ext}$ naturally divides the $\Sigma_{\rm SFR}$–$\Sigma_{\rm gas}$ plane into two regimes of SF activity when a linear relation such as $\Sigma_{\rm SFR} \propto \Sigma_{\rm mol}$ is assumed, according to whether $R_{\rm mol} > 1$ or <1. In this picture, it is the transition from atomic- to molecular-dominated gas which causes the change of slope in the $\Sigma_{\rm SFR}$–$\Sigma_{\rm gas}$ relation, rather than the stability of the disc. Note that the empirical SF laws discussed above attempt to describe the SF activity in galaxies on scales larger than $\sim$500 pc, averaging over representative volumes of the interstellar medium (ISM) including both star-forming clouds and intercloud gas (e.g. Fumagalli, Krumholz & Hunt 2010; Onodera et al. 2010; Schruba et al. 2010).

Even though the quality of the observational data has improved the characterization of the SF law, there is still uncertainty regarding the main physical mechanism that governs the SFR in galaxies. Possibilities currently under discussion include the formation of molecules on dust grains in turbulence-regulated giant molecular clouds (GMCs; Krumholz & McKee 2005; Krumholz, McKee & Tumlinson 2009b) and collisions of GMCs in shearing discs (Tan 2000; Schaye 2004; Silk & Norman 2009; see McKee & Ostriker 2007, for a comprehensive review of the theory of SF activity). Direct comparisons of empirical and theoretical SF models with observations by Leroy et al. (2008) revealed that thresholds of large-scale stability, as proposed by K98, or a simple dependence on the orbital or free-fall time-scales as in Tan (2000), do not offer a good explanation for the observed $\Sigma_{\rm SFR} \propto \Sigma_{\rm mol}$ relation. On the other hand, for a suitable choice of parameters, the Krumholz et al. (2009b) SF law is able to reproduce the observational results described above fairly well. The nature of the physical processes underlying the global SF law could be identified by resolving individual GMCs and SF regions in the Milky Way and other galaxies. Ongoing observations with *Herschel* and future telescopes such as Atacama Large Millimeter Array (ALMA) and the Square Kilometre Array (SKA) will help us to better characterize the properties of individual SF regions, and to test the applicability of locally derived SF laws at higher redshifts.

In this paper, we implement new recipes for SF in the GALFORM semi-analytical model of galaxy formation in a Λ cold dark matter (ΛCDM) cosmology (Cole et al. 2000). We focus on the empirical laws proposed by K98 and BR06 and the theoretical model of Krumholz et al. (2009b). Our aim is to identify the galaxy observable properties which can distinguish between different SF prescriptions, and also to identify behaviour which is common to different SF laws. To do this, we insert the new SF prescriptions into existing GALFORM models (Baugh et al. 2005, hereafter Bau05; Bower et al. 2006, hereafter Bow06) *without* changing any other model parameters to achieve a new 'best' fit to observations (see Cole et al. 2000 and Bower et al. 2010, for discussions of fitting model parameters). We first study predictions for the cosmic SFR evolution and then for the evolution of the cold gas content of galaxies and their level of SF activity, which are very sensitive to this choice. An important result obtained in this work is that the study of the SFR in galaxies of different stellar masses offers a useful constraint on the choice of SF law. New radio telescopes such as Meer Karoo Array Telescope (MeerKAT) (Booth et al. 2009), Australian Square Kilometer Array Pathfinder (ASKAP) (Johnston et al. 2008) and SKA (Schilizzi, Dewdney & Lazio 2008) will measure the abundance of H I in the Universe and its evolution. ALMA will soon begin to probe both the molecular gas contents and dust-obscured SFRs in high-redshift galaxies. The predictions made in this paper can be used in conjunction with these future observations to constrain the physical processes that trigger SF in galaxies.

This paper is organized as follows. In Section 2, we present the GALFORM model and the two variants we use to study the impact of applying different SF laws, pointing out the main differences and similarities between them. We also describe the SF laws tested. In Section 3 we study the impact of changing the SF law on the evolution of the cosmic SFR density. Section 4 examines the evolution of the cold gas content of galaxies, and we discuss the physics that shapes its evolution. In Section 5, we present a new means to distinguish between different SF laws, namely the shape of the sequences in the SFR–stellar mass plane, and compare with available observations. Finally, in Section 6, we discuss our results in the context of future surveys and observations. The appendices cover the details of the numerical scheme used to implement the new SF laws, some details of the SF laws used and present some predictions for observables which are insensitive to the choice of SF law.

2 MODELLING THE STAR FORMATION ACTIVITY IN GALAXIES

We first give an overview of the GALFORM galaxy formation model (Section 2.1), before describing the SF recipes used in GALFORM (Section 2.2). In Section 2.3 we outline the new SF laws (see Appendix A for a description of the numerical implementation of these laws and Appendix B for some more details of the SF laws).

2.1 The galaxy formation model

We study the impact on the galaxy population of applying different SF laws in the GALFORM semi-analytic model of galaxy formation (Cole et al. 2000; Benson et al. 2003; Bau05; Bow06; Lacey et al. 2008; Benson & Bower 2010). GALFORM models the main physical processes that shape the formation and evolution of galaxies: (i) the collapse and merging of DM haloes; (ii) the shock heating and radiative cooling of gas inside DM haloes, leading to the formation of galactic discs; (iii) quiescent SF in galactic discs; (iv) feedback from supernovae (SNe), from active galactic nucleus (AGN) heating

and from photoionization of the intergalactic medium; (v) chemical enrichment of stars and gas and (vi) galaxy mergers driven by dynamical friction within common DM haloes, which can lead to the formation of spheroids and trigger bursts of SF (for reviews see Baugh 2006 and Benson 2010). Galaxy luminosities are computed from the predicted SF and chemical enrichment histories using a stellar population synthesis model. Dust extinction is calculated self-consistently from the gas and metal contents of each galaxy and the predicted scalelengths of the disc and bulge components using a radiative transfer model (see Cole et al. 2000 and Lacey et al. 2011).

We consider the models published by Bau05 and Bow06. The main successes of the Bow06 model are the reproduction of the observed break in the galaxy luminosity function (LF) at $z = 0$ in the b_J and K bands, the observational inferred evolution of the stellar mass functions up to $z \approx 5$, the bimodality in the colour–magnitude relation and the abundance and properties of red galaxies (Gonzalez-Perez et al. 2009). The Bau05 model likewise matches b_J- and K-band LFs at $z = 0$, but also the number counts and redshift distribution of submillimetre-selected galaxies (see also González et al. 2011), disc sizes (Almeida, Baugh & Lacey 2007; González et al. 2009), the evolution of Lyα emitters (Le Delliou et al. 2006; Orsi et al. 2008), counts, redshift distributions and LFs of galaxies selected in the mid- and far-IR (Lacey et al. 2008, 2010) and the Lyman-break galaxy LF at redshifts $z = 3$–10 (Lacey et al. 2011).

We refer the reader to the original papers for full details of the Bau05 and Bow06 models. Discussions of the differences between the models can be found in Almeida et al. (2007), González et al. (2009), Gonzalez-Perez et al. (2009) and Lacey et al. (2011). Briefly, the main differences between the models are the following.

(i) The SF time-scale in galactic discs. The Bow06 model adopts a parametrization for the SF time-scale which depends on the global dynamical time-scale of the disc, whereas the Bau05 model adopts a time-scale which depends only on the disc circular velocity (see Section 2.1). Consequently, high-redshift galaxies in the Bau05 model have longer SF time-scales than those in the Bow06 model and are therefore more gas rich. This leads to more SF activity in bursts in the Bau05 model compared to the Bow06 model.

(ii) The stellar initial mass function (IMF) is assumed to be universal in the Bow06 model, with the Kennicutt (1983) IMF adopted. The Bau05 model assumes two IMFs, a top-heavy IMF during SBs and a Kennicutt IMF during quiescent SF in discs. Defining the IMF slope x through $\mathrm{d}N/\mathrm{d}\ln m \propto m^{-x}$, the Kennicutt IMF has $x = 0.4$ below $m = 1\ \mathrm{M}_\odot$ and $x = 1.5$ at higher masses, while the top-heavy IMF has $x = 0$.

(iii) The gas expelled from galaxies by SN feedback is assumed to be reincorporated into the hot halo after a few dynamical times in the Bow06 model. In the Bau05 model, this happens only after the DM halo doubles its mass. This time, called the halo lifetime, is usually much longer than the dynamical time of the halo.

(iv) In order to reproduce the bright-end of the LF, the Bau05 model invokes SNe-driven superwinds with a mass ejection rate proportional to the SFR (note that the expelled material is not reincorporated into any subsequent halo in the DM merger tree). The Bow06 model includes AGN feedback to switch off the cooling flow in haloes where the central black hole (BH) has an Eddington luminosity exceeding a multiple of the cooling luminosity (the multiple being a model parameter).

(v) The Bow06 model includes disc instabilities (e.g. Mo, Mao & White 1998) as an extra mechanism to trigger bursts of SF and to make spheroids, and hence to build BH mass (Fanidakis et al. 2010).

We use halo merger trees extracted from the Millennium cosmological N-body simulation (Springel 2005) in the Bow06 model and Monte Carlo trees in the Bau05 model, as in the original models. We use the Monte Carlo algorithm of Parkinson, Cole & Helly (2008) to generate DM merger trees for the Bau05 model from that of Cole et al. (2000). González et al. (2011) tested that changing the tree-generation scheme does not significantly change the model predictions. The Bau05 model adopts a ΛCDM cosmology with a present-day matter density parameter, $\Omega_\mathrm{m} = 0.3$, a cosmological constant, $\Omega_\Lambda = 0.7$, a baryon density, $\Omega_\mathrm{baryons} = 0.04$, a Hubble constant, $h = 0.7$, and a power spectrum normalization of $\sigma_8 = 0.93$. The Bow06 model is set in the Millennium simulation which has the following cosmology: $\Omega_\mathrm{m} = \Omega_\mathrm{DM} + \Omega_\mathrm{baryons} = 0.25$ (giving a baryon fraction of 0.18), $\Omega_\Lambda = 0.75$, $\sigma_8 = 0.9$ and $h = 0.73$. The resolution of the N-body simulation is fixed at a halo mass of $1.72 \times 10^{10}\, h^{-1}\, \mathrm{M}_\odot$. In the Bau05 model, Monte Carlo merger histories are generated for a grid of halo masses. The grid is laid down at selected redshifts, sampling haloes in a fixed dynamic range of mass which scales as $(1 + z)^{-3}$ to approximately track the break in the mass function. The minimum halo mass for merger trees at $z = 0$ is $10^9\, h^{-1}\, \mathrm{M}_\odot$. The Monte Carlo trees therefore include lower mass haloes than in the N-body case.

2.2 The original star formation laws in GALFORM

The original GALFORM models used a parametric SF law to compute quiescent SFR at each time-step (Cole et al. 2000):

$$\psi = \frac{M_\mathrm{cold}}{\tau_\star}, \tag{1}$$

where M_cold is the total cold gas mass in the galactic disc and $\tau_\star$ is the time-scale for the SF activity which may depend on galaxy parameters but not on the gas mass. This choice was motivated by the observations of K98 (see Bell et al. 2003). The SF time-scale in equation (1) was parametrized by Cole et al. (2000) as

$$\tau_\star = \frac{\tau_\mathrm{disc}}{\epsilon_\star}\,(V_\mathrm{disc}/V_0)^{\alpha_\star}, \tag{2}$$

where $V_0 = 200\,\mathrm{km\,s^{-1}}$, V_disc is the disc circular velocity at the half-mass radius, $\tau_\mathrm{disc} = r_\mathrm{disc}/V_\mathrm{disc}$ is the disc dynamical time-scale, and $\epsilon_\star$ and $\alpha_\star$ are free parameters, with values originally chosen to reproduce the gas-to-luminosity ratio observed in local spiral galaxies (Cole et al. 2000). Bow06 adopted values of $\epsilon_\star = 0.0029$ and $\alpha_\star = -1.5$, mainly to reproduce the galaxy LF, without particular reference to the cold gas to luminosity ratio (see Kim et al. 2010).

In the Bau05 model a different SF time-scale was adopted, in order to reduce the amount of quiescent SF activity at high redshift, thereby allowing more SF in bursts. The recipe used in the Bau05 model is

$$\tau_\star = \tau_0\,(V_\mathrm{disc}/V_0)^{\alpha_\star}, \tag{3}$$

where $V_0 = 200\,\mathrm{km\,s^{-1}}$, τ_0 and α are free parameters set to $\tau_0 = 8\,\mathrm{Gyr}$ and $\alpha_\star = -3$, in order to match the local gas mass to luminosity ratio (see Power, Baugh & Lacey 2010).

During SBs caused by galaxy mergers and, in the case of the Bow06 model, also by disc instabilities, the available reservoir of cold gas is assumed to be consumed in the SB event with a finite duration. The SF time-scale in bursts is taken to be $f_\mathrm{dyn}\,\tau_\mathrm{bulge}$, with

a floor value $\tau_{*\mathrm{burst,min}}$, with τ_{bulge} being the bulge dynamical time. Bau05 adopted $f_{\mathrm{dyn}} = 50$ and $\tau_{*\mathrm{burst,min}} = 0.2\,\mathrm{Gyr}$, while Bow06 used $f_{\mathrm{dyn}} = 2$ and $\tau_{*\mathrm{burst,min}} = 0.005\,\mathrm{Gyr}$.

The need for two free parameters in equations (2) and (3) reflects a lack of understanding of the physics of SF. New, high-resolution, spatially resolved data reveal that an SF law of the form of equation (1) with $\tau_\star$ independent of the gas density results in a poor fit to the observations (Leroy et al. 2008). It is necessary to revisit the SF law used in GALFORM and to study more consistent ways to characterize the SF in galaxies.

2.3 The new star formation laws

Here we summarize the three new forms of SF law that we implement for quiescent SF in GALFORM. These are the empirical relations of (i) K98 and (ii) BR06, and (iii) the theoretical model of Krumholz et al. (2009b). The observational situation for SBs is less clear than it is for discs, so we retain the original GALFORM prescription for the SF time-scale in SB (see above).

2.3.1 The Kennicutt–Schmidt law

Following the pioneering work of Schmidt (1959), observational studies have found that the surface density of SF (Σ_{SFR}) correlates with the projected gas density (Σ_{gas}). K98 fitted the relation

$$\Sigma_{\mathrm{SFR}} = A\,\Sigma_{\mathrm{gas}}^{N}, \tag{4}$$

where $N = 1.4 \pm 0.15$ and $A = 0.147$[1] when Σ_{gas} and Σ_{SFR} are measured in $\mathrm{M_\odot\,pc^{-2}}$ and $\mathrm{M_\odot\,pc^{-2}\,Gyr^{-1}}$, respectively. This relation holds over five orders of magnitude in SFR and gas surface density, but shows a break to a steeper relation in the outer regions of spirals and in dwarf galaxies (K89; K98; Bigiel et al. 2008; Leroy et al. 2008).

The Kennicutt–Schmidt SF law combines the power-law dependence of the SFR on Σ_{gas} at high gas densities with a cut-off in SF below a critical gas surface density, Σ_{crit}, as observed at low gas surface densities by K89 and Martin & Kennicutt (2001). The Σ_{crit} threshold is motivated by the Toomre (1964) stability criterion. In the case of a thin isothermal gas disc with a flat rotation curve, the critical surface density for gravitational instability of axisymmetric perturbations is given by

$$\Sigma_{\mathrm{crit}} = \frac{\sqrt{2}}{Q_{\mathrm{crit}}\,\pi G}\,\sigma_{\mathrm{g}}\,\frac{V}{R}, \tag{5}$$

where Q_{crit} is a dimensionless constant $\sim$1 and σ_{g} is the velocity dispersion of the gas (see Appendix B1 for a derivation of equation 5). We adopt $\sigma_{\mathrm{g}} = 10\,\mathrm{km\,s^{-1}}$ consistent with the observations of Leroy et al. (2008). K98 found $Q_{\mathrm{crit}} \approx 2.5$ (after scaling by our choice of σ_{g}, which is larger than the original value adopted by K98). By adopting these values, we calculate Σ_{crit}, and suppress SF at radii in which $\Sigma_{\mathrm{gas}} < \Sigma_{\mathrm{crit}}$.

We will consider two forms of the Kennicutt–Schmidt law, with and without SF suppression below Σ_{crit} (equation 5). We denote these SF laws as KS.thresh (with suppression) and KS (without suppression).

2.3.2 The Blitz & Rosolowsky model: molecular gas fraction determined by pressure

BR06 based their SF law on two observationally motivated considerations.

(i) Observations in the IR and at millimetre wavelengths suggest that stars form in dense gas environments, namely GMCs (see Solomon & Vanden Bout 2005, for a review). BR06 assume that the SFR is set by the surface density of molecular gas[2] Σ_{mol}, with a proportionality factor (given as an inverse time-scale) ν_{SF}:

$$\Sigma_{\mathrm{SFR}} = \nu_{\mathrm{SF}}\,\Sigma_{\mathrm{mol}}. \tag{6}$$

(ii) BR06 propose that the ratio of molecular to atomic hydrogen gas, R_{mol}, is given by a power law in the internal hydrostatic pressure in a galactic disc, P_{ext}:

$$R_{\mathrm{mol}} \equiv \frac{\Sigma(\mathrm{H_2})}{\Sigma(\mathrm{H\,I})} = \left(\frac{P_{\mathrm{ext}}}{P_0}\right)^{\alpha}. \tag{7}$$

BR06 found that the observed molecular-to-atomic ratios in their galaxy sample were well fitted using values of $\log(P_0/k_{\mathrm{B}}\,[\mathrm{cm^{-3}\,K}]) = 4.54 \pm 0.07$ and $\alpha = 0.92 \pm 0.07$. Leroy et al. (2008) found similar values using a somewhat larger sample. The hydrostatic pressure in disc galaxies at the mid-plane is calculated following Elmegreen (1993; see Appendix B2 for details).

The original SF law of equation (6) can hence be rewritten in terms of the total gas surface density and the molecular-to-total hydrogen ratio, $f_{\mathrm{mol}} = \Sigma_{\mathrm{mol}}/\Sigma_{\mathrm{gas}} = R_{\mathrm{mol}}/(R_{\mathrm{mol}} + 1)$, as

$$\Sigma_{\mathrm{SFR}} = \nu_{\mathrm{SF}}\,f_{\mathrm{mol}}\,\Sigma_{\mathrm{gas}}. \tag{8}$$

We consider two cases for ν_{SF}: (i) a constant value $\nu_{\mathrm{SF}} = \nu_{\mathrm{SF}}^0 = 0.525 \pm 0.25\,\mathrm{Gyr^{-1}}$ (Leroy et al. 2008),[3] which gives a linear dependence of Σ_{SFR} on Σ_{gas} at high surface densities, and (ii) a surface density dependent ν_{SF} given by

$$\nu_{\mathrm{SF}} = \nu_{\mathrm{SF}}^0\left[1 + \left(\frac{\Sigma_{\mathrm{gas}}}{\Sigma_0}\right)^{q}\right], \tag{9}$$

where $\Sigma_0 = 200\,\mathrm{M_\odot\,pc^{-2}}$ and $q = 0.4$ are chosen to recover the K98 law at high gas surface densities, and the steepening seen in the Σ_{SFR}–Σ_{gas} relation when SBs are included (Bigiel et al. 2008). The surface density Σ_0 is similar to the typical surface densities of individual GMCs in spiral galaxies, so the transition to the steeper dependence could be interpreted as happening when these clouds start to overlap. We refer to the SF law with a constant ν_{SF} as BR and to the second form, where $\nu_{\mathrm{SF}} = \nu_{\mathrm{SF}}(\Sigma_{\mathrm{gas}})$, as BR.nonlin.

2.3.3 The Krumholz, McKee & Tumlinson model: turbulence-regulated star formation activity

Krumholz, McKee & Tumlinson (2009b, hereafter KMT09) calculate ν_{SF} and f_{mol} of equation (8) for a spherical cloud with SF regulated by supersonic turbulence.

[1] We have rescaled the value of A to account for the difference between the Salpeter IMF assumed by K98 and the Kennicutt IMF used in our model for quiescent SF. The SFRs used in K98 were inferred from Hα luminosities, and for a fixed Hα luminosity, the SFR on assuming a Kennicutt IMF is 0.91 times that inferred on adopting a Salpeter IMF. Note also that we always use gas surface densities including helium, assuming a hydrogen mass fraction of 74 per cent.

[2] Note that we include the associated helium in the molecular gas mass, in the same way as for the total gas mass.

[3] Leroy et al. (2008) derived their SFRs from a calibration using far-UV luminosities, assuming a Kroupa (2001) IMF. For the Kennicutt IMF, we infer SFRs 1.02 times larger. For simplicity, we do not apply this correction factor, since it is so close to 1.

KMT09 assume that $f_{\rm mol}$ is determined by the balance between the photodissociation of H_2 molecules by the interstellar far-UV radiation and the formation of molecules on the surface of dust grains. Krumholz, McKee & Tumlinson (2009a) calculated $f_{\rm mol}$ theoretically for spherical cloud, and showed that it is approximately a function of the gas surface density of the atomic–molecular complex (or GMC) $\Sigma_{\rm comp}$ and of the gas metallicity Z (see also McKee & Krumholz 2010). We use equation (2) from KMT09 for $f_{\rm mol}(\Sigma_{\rm comp}, Z)$. KMT09 assume that the surface density of the GMC is related to that of the ISM on larger scales by $\Sigma_{\rm comp} = c\Sigma_{\rm gas}$, where the clumping factor $c \geq 1$ is a free parameter, which is not predicted by the model. It is implicitly assumed that the fraction of the ISM in GMCs is equal to the molecular fraction within a single GMC. Given that the KMT09 formula predicts that $f_{\rm mol} \rightarrow 0$ in very metal poor environments, we assume that a minimum $f_{\rm mol}^{\rm min} = 10^{-4}$ characterizes pristine gas at very high redshift (see Appendix B3.1 for more details).

KMT09 define $\nu_{\rm SF}$ as the inverse of the time-scale required to convert all of the gas in a cloud into stars, and obtain it from a theoretical model of turbulent fragmentation (Krumholz & McKee 2005). The parameter $\nu_{\rm SF}$ in a cloud depends on the cloud surface density, $\Sigma_{\rm cl}$. KMT09 assume that $\Sigma_{\rm cl}$ is a constant (Σ_0) in normal spiral galaxies, but increases in higher density environments, so that $\Sigma_{\rm cl} = \max[\Sigma_0, \Sigma_{\rm gas}]$ (see Appendix B3.2 for more details). Combining all of these ingredients, KMT09 obtain

$$\nu_{\rm SF}(\Sigma_{\rm gas}) = \nu_{\rm SF}^0 \times \left(\frac{\Sigma_{\rm gas}}{\Sigma_0}\right)^{-0.33} \quad \text{for} \quad \Sigma_{\rm gas} < \Sigma_0 \tag{10}$$

$$= \nu_{\rm SF}^0 \times \left(\frac{\Sigma_{\rm gas}}{\Sigma_0}\right)^{0.33} \quad \text{for} \quad \Sigma_{\rm gas} > \Sigma_0, \tag{11}$$

with $\nu_{\rm SF}^0 = 0.38\,{\rm Gyr}^{-1}$ and $\Sigma_0 = 85\,{\rm M}_\odot\,{\rm pc}^{-2}$. The molecular fraction $f_{\rm mol}(c\Sigma_{\rm gas}, Z)$ contains the dependence on the clumping factor c. The KMT09 SF model thus predicts three regimes of SF (qualitatively similar to the BR.nonlin model): (i) regions with low gas surface densities and hence low molecular gas fractions, which produce steeper SF relations; (ii) an intermediate-density regime characterized by constant GMC surface densities and (iii) a high-density regime where there is an increase in the GMC density. This model is able to reproduce reasonably well the observed trend of $\Sigma_{\rm SFR}$ with $\Sigma_{\rm gas}$ in nearby galaxies on adopting $c \approx 5$, roughly consistent with observed overdensities of molecular gas complexes (Rosolowsky & Blitz 2005; Schuster et al. 2007). Hereafter we will refer to this SF law as KMT.

3 THE EVOLUTION OF THE SFR DENSITY

Our aim is to investigate the impact on galaxy properties of changing the SF law over a wide range of redshifts, and to compare the new predictions with those of the original Bau05 and Bow06 models. To do this, we leave the parameter values for processes other than the SF law unchanged, to isolate the effects of changing the SF prescription. We apply the new SF laws consistently throughout the galaxy formation calculation (see Appendix C for an illustration of applying the SF laws to the original models over a single time-step).

Fig. 1 shows the evolution of the cosmic SFR density (top), distinguishing between quiescent (middle) and burst (bottom) SF modes, for the Bau05 (left) and the Bow06 (right) models. In the Bau05 model, the peak in SF activity is at $z \approx 2.5$. The peak location (though not its height) is somewhat sensitive to the choice of SF law, moving to higher redshift in the variant models. The extreme cases are the KS and KS.thresh SF laws, in which the peak shifts to $z \approx 3.5$. In the case of the KMT and BR.nonlin laws, the peak moves slightly to $z \approx 2.8$, while the BR law gives a very similar SFR density evolution to the original Bau05 model. The change in the location of the SFR density peak is driven by the change in the level of quiescent SF activity. SF laws that produce higher SFR densities in the quiescent mode at high redshift (i.e. KS, KS.thresh, KMT, BR.nonlin) are characterized by an SFR–gas density correlation $\Sigma_{\rm SFR}$–$\Sigma_{\rm gas}$ steeper than linear (e.g. $N > 1$ in equation 4). A consequence of the larger quiescent SFR at high redshifts is less cold gas available to fuel SBs, and so the SFR density in the burst mode drops.

In the Bow06 model (right-hand panels in Fig. 1), the evolution of the total SFR density is largely unaffected by the choice of SF law even though the relative importance of the quiescent and burst SF modes changes by more than one order of magnitude. This is due to the inclusion of SBs triggered by disc instabilities (Section 2). The smaller SFR density in the quiescent mode relative to the original model when using the BR, BR.nonlin and KMT SF laws (middle panel) leads to significant amounts of cold gas in galaxy discs. This results in a higher frequency of unstable discs and gas-rich mergers, and also more prominent SBs due to the larger gas reservoirs. This increase in SB activity compensates for the lower quiescent activity. In the case of the KS and KS.thresh laws, the slightly smaller SFR density (by $\approx$−0.1 dex) in the quiescent mode is not offset by an increase in the SF activity from disc instabilities. This is because the condition for a disc to become dynamically unstable is only weakly dependent on mass ($\propto M_{\rm disc}^{-1/2}$). Hence, a substantial change in disc mass is needed to make a galaxy unstable, and on average the change in disc mass is less than 0.1 dex for the KS and the KS.thresh laws, while for the other SF laws it is at least 0.4 dex. Remarkably, all of the new SF laws produce peaks of burst and quiescent SF activity separated by at least $\Delta z \approx 1$, while in the original Bow06 model, the peaks overlap.

The differences on applying the new SF laws in the Bau05 and Bow06 models indicate the role of physical processes other than quiescent SF in shaping the evolution of galaxies, e.g. disc instabilities, and support our decision to leave the other model parameters unchanged. However, there are remarkable similarities between the predictions which result on using different SF laws. Even though the total density of SF activity is unchanged, the relative importance of the burst and quiescent modes depends sensitively on the choice of SF law, due mainly to the change in the cold gas content of galaxies (see Section 4). The insensitivity of the total SFR density to the choice of SF law has been noted in previous work (e.g. Stringer & Benson 2007; Dutton, van den Bosch & Dekel 2010; Schaye et al. 2010). This can be understood as resulting from the SFR (combined with the rate of gas ejection from galaxies due to SN feedback, which is proportional to the SFR) on average adjusting to balance the rate of accretion of cooling gas. The SFR will tend to adjust in this way whenever the gas consumption time-scale $\tau_{\rm SF} \equiv M_{\rm cold}/{\rm SFR}$ is less than the age of the universe at that redshift. A direct consequence of this interplay between the modes of SF is the insensitivity of the optical and near-IR galaxy LF and optical colours to the choice of SF law (see Appendix D for a comparison of the predicted LFs and other galaxy properties when using different SF laws).

4 COLD GAS MASS CONTENT OF GALAXIES

The cold gas mass content of galaxies is sensitive to the choice of SF law, since this determines the rate at which gas is converted into

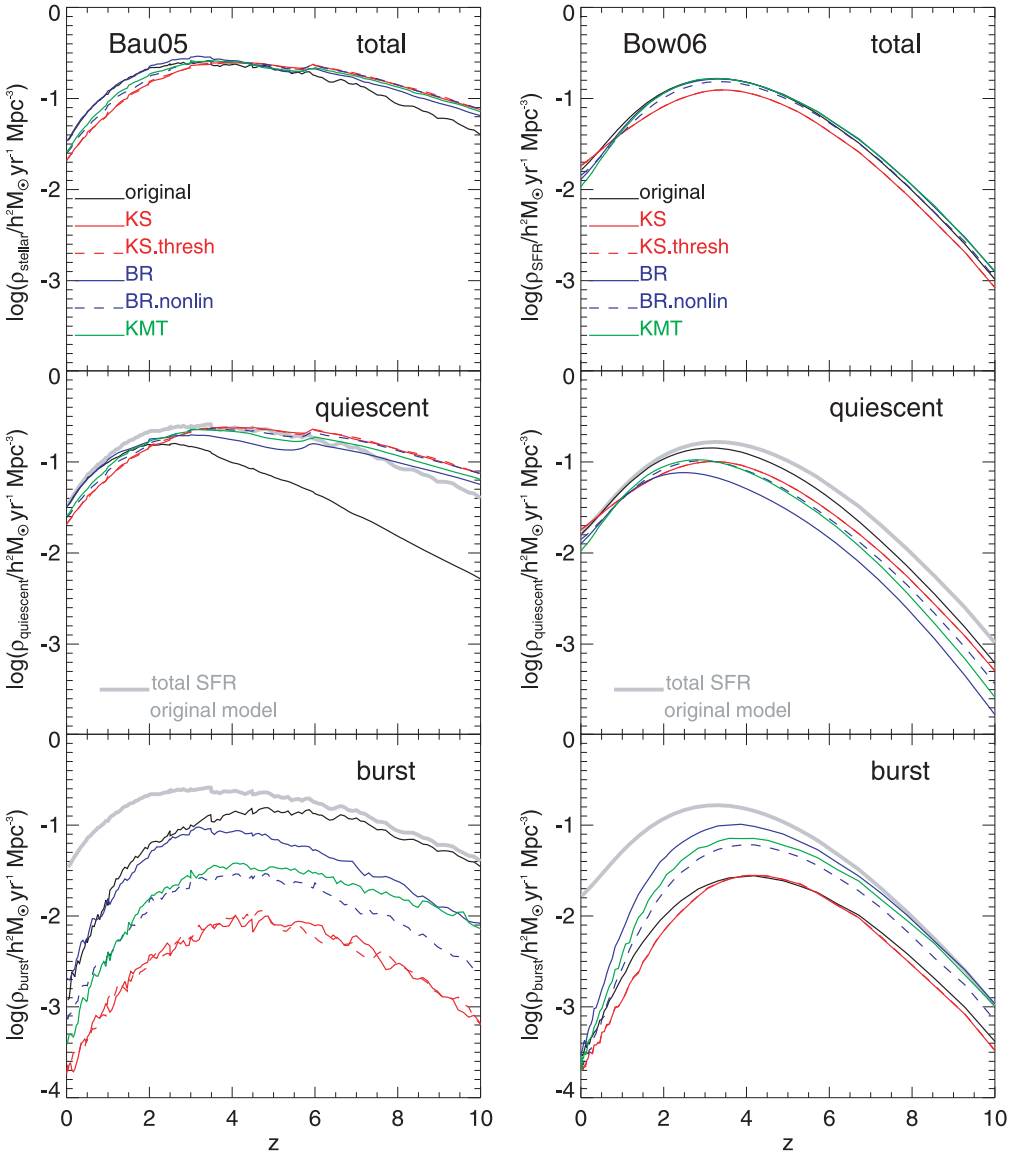

Figure 1. The evolution of the cosmic SFR per unit volume. The left-hand panels show the Bau05 model and its variants, and the right-hand panels show the Bow06 model. The top row shows the total SFR, the middle panels show the quiescent SF and the bottom panels the SF in bursts. For reference, in the middle and bottom panels the total SFR density in the original models is shown by a thick grey solid line.

stars. Here we focus on three separate observational probes of gas: the cold gas mass function (CMF), the evolution of the cold gas density of the universe and the gas-to-luminosity ratio in galaxies.

4.1 Cold gas mass function

Fig. 2 shows the CMF at different redshifts for the original models and with different SF laws. The observed $z = 0$ CMF of Zwaan et al. (2005) is plotted to highlight evolution. Note that the observed CMF plotted here is derived from the observed H I mass function assuming a constant $H_2/H\,I$ ratio of 0.4 and a hydrogen mass fraction $X = 0.74$ (Section 2.3.1) to convert the H I measurements into cold gas masses (Baugh et al. 2004; Kim et al. 2010; Power et al. 2010).

The Bau05 model is in quite good agreement with the observed CMF, except at the lowest gas masses. The parameters in the original model were chosen to match the gas-to-luminosity ratios discussed in Section 4.3. The modified SF laws all lead to poorer agreement with observations. On the other hand, the original Bow06 model is in poor agreement with the observed CMF. Some of the variant SF laws in this case lead to better agreement with the observed CMF.

Most of the changes in the CMF with the new SF laws can be understood as resulting from the changed SF time-scales in discs, defined as $\tau_{SF} = M_{cold}/SFR$. (Note that τ_{SF} would be equal to the gas depletion time-scale if there was no accretion of fresh gas from cooling, no ejection of gas by SN feedback and no recycling of gas to the ISM by dying stars.) Since the treatment of gas cooling in haloes is unchanged, accretion rates of cold gas on to discs are also essentially unchanged, so an increase in the SF time-scale τ_{SF} leads to larger cold gas masses in discs and vice versa. The new SF laws depend on galaxy properties such as the radius, stellar mass and gas metallicity in different ways from the old laws. Furthermore, all of the new SF laws are non-linear in cold gas mass, at least in the low gas density regime, so that τ_{SF} always increases if M_{cold} becomes

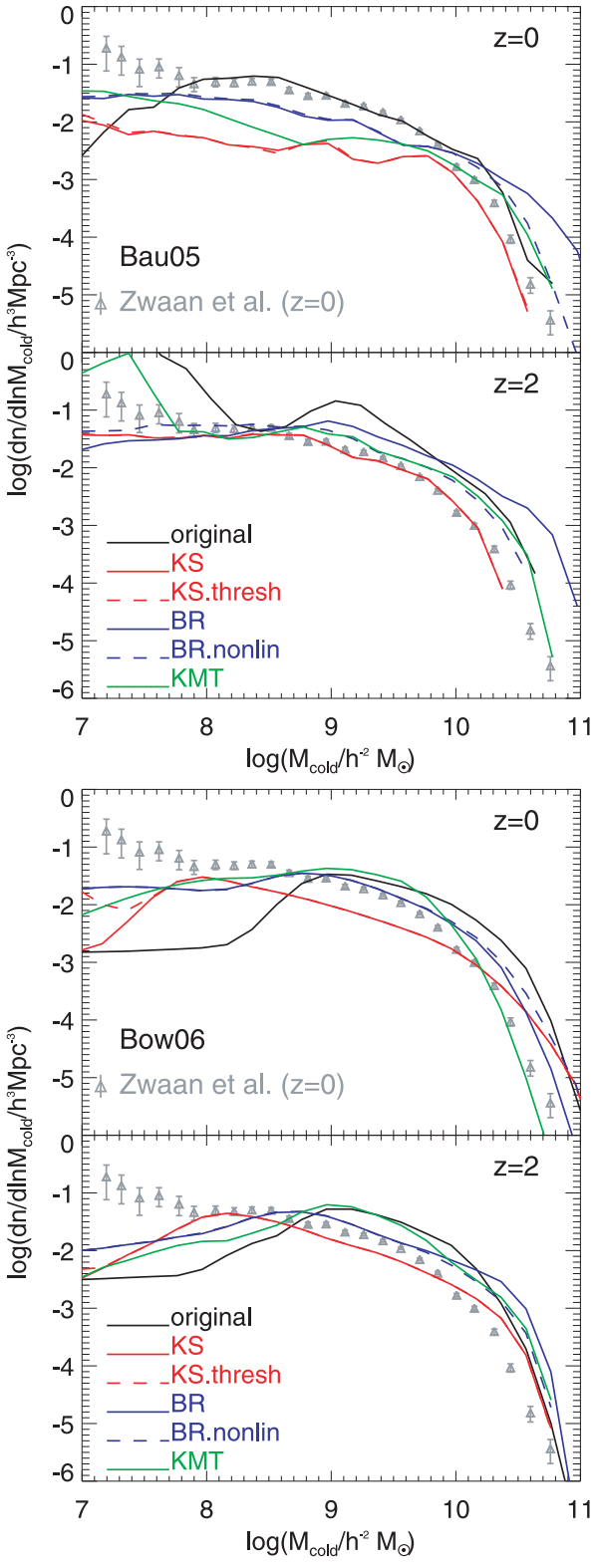

Figure 2. The CMFs at $z = 0$ and 2 for the Bau05 (upper two panels) and the Bow06 (lower two panels) models and for the different forms of the SF law. The line colours and styles are as in Fig. 1. For reference, the observational estimate of the $z = 0$ CMF from Zwaan et al. (2005) is shown using grey symbols in all panels. A constant $H_2/H\,I$ ratio of 0.4 has been assumed to convert the H I observations into cold gas masses.

low enough, in contrast to the original SF laws, for which τ_{SF} is independent of the remaining gas mass. As a result, the changes in gas content due to changing the SF law themselves depend on the galaxy mass and redshift (see Appendix C for the change in SFR with galaxy mass and redshift for different SF laws).

SBs triggered by disc instabilities have a bearing on gas content in the Bow06 model. Changing the SF law can lead to changes in the total disc mass, making the disc more prone to instabilities if the total mass is larger. Following an instability, all of the gas is consumed in an SB. Thus, paradoxically, longer SF time-scales in discs can lead to *lower* final gas contents in some cases. SBs in the Bau05 model are triggered only by galaxy mergers, and the frequency of these is essentially unaffected by changes in the gas content of galaxies.

In the Bau05 model, the SF time-scales are in most cases shorter with the new SF laws, and so the CMF is also lower at most gas masses. For the Bow06 model, the results of changing the SF law are more mixed, although the CMF is generally lower at intermediate gas masses. An interesting effect appears at low gas masses, where in all cases the number density is larger than with the original SF laws, bringing the models closer to the observational data at $z = 0$. This results from the new SF laws being non-linear in the cold gas mass, so that the gas is depleted less rapidly when the mass becomes very small than with the original (linear) SF laws. The effects of halo mass resolution are more severe for the Bow06 model, which uses N-body merger trees from the Millennium simulation. This is what causes the turndown in the CMF for $M_{\rm cold} \lesssim 10^9\,h^{-2}\,{\rm M}_\odot$.

The high-mass end of the CMF in the Bow06 model evolves significantly from $z = 2$ to 0 due to the longer SF time-scales at lower redshifts (see equation 2). With the new SF laws, this evolution is weaker, due in part to the higher frequency of disc instabilities triggering SBs which consume the gas.

The evolution of the CMF is therefore a useful diagnostic to distinguish between the SF laws, since they lead to changes that are differential with galaxy mass.

4.2 Global cold gas density evolution

The evolution of the global cold gas density, $\rho_{\rm cold}$, is shaped by the same processes as the CMF. Fig. 3 shows $\rho_{\rm cold}$ as a function of redshift for the Bau05 (top panel) and Bow06 (bottom panel) models and the variants with new SF laws. For reference, grey symbols show different observations as listed in the legends. In general, all the new SF laws predict lower $\rho_{\rm cold}$ than the original models across the whole redshift range.

In the Bau05 model, the reduced $\rho_{\rm cold}$ with the new SF laws is due to the shorter quiescent SF time-scales in low and intermediate cold gas mass objects (see right-hand panels of Fig. C1). In general, the shorter the quiescent SF time-scale (on average), the smaller the $\rho_{\rm cold}$ compared to the original model. Note that the jump of $\rho_{\rm cold}$ at $z \approx 6$ in the Bau05 model is due to the assumed reionization redshift $z_{\rm reion} = 6$ (Section 6.1).

On the other hand, in the Bow06 model the BR, BR.nonlin and the KMT SF laws at very high redshift (i.e. $z \geq 6$) give similar $\rho_{\rm cold}$ to the original model, mainly due to the compensation between quiescent and burst SF activity. The BR, BR.nonlin and the KMT SF laws give reasonable agreement with the observed $\rho_{\rm cold}$ at $z = 0$, improving over the original model.

The Bow06 model shows a more rapid decrease of $\rho_{\rm cold}$ with increasing redshift than the Bau05 model. This results in part from the stronger SNe feedback in the Bow06 model, but is also due to the difference in the mass resolution of the halo merger trees used

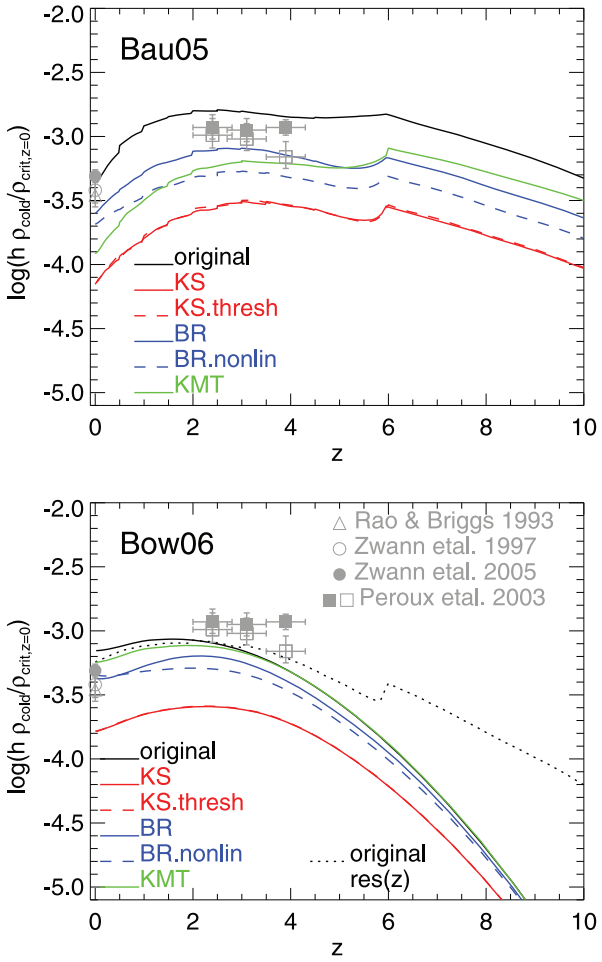

Figure 3. The cold gas mass density in the universe, $\rho_{\rm cold}$, in units of the critical density at $z = 0$, $\rho_{{\rm crit},z=0}$, as a function of redshift. The results for the original Bau05 and Bow06 models and with the new SF laws are shown in the top and bottom panels, respectively. Grey symbols show observational results from Zwaan et al. (1997, 2005; open and filled circles, respectively), Rao & Briggs (1993; open triangles) and Péroux et al. (2003; open and filled squares). For the latter, open symbols indicate the cold gas density inferred from damped Lyα systems, while filled symbols include a correction for gas clouds with lower column density than originally detected. The dotted line in the bottom panel shows the effect of changing the halo mass resolution from the default values, as discussed in the text.

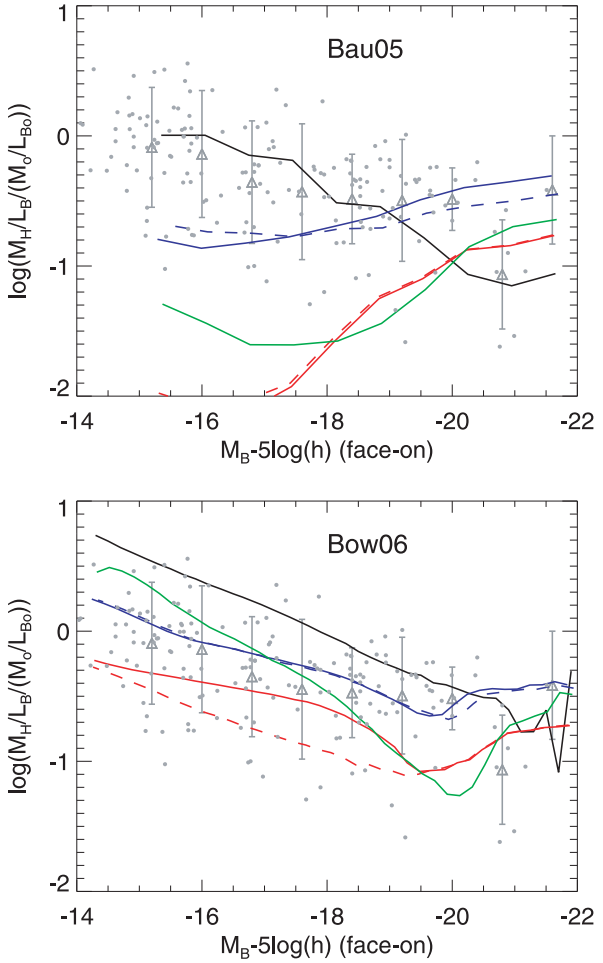

Figure 4. Hydrogen gas mass to luminosity ratios, $M_{\rm H}/L_B$, as a function of B-band magnitude for late-type galaxies. Late-type galaxies in the model are those with a bulge-to-total luminosity ratio in the B band of $B/T \leq 0.4$. The Bau05 and Bow06 models are shown in the top and bottom panels, respectively. The line colours and styles which represent the different SF laws are the same as in Fig. D1. For clarity we only show the median of each model. Observational results from Huchtmeier & Richter (1988) and Sage (1993) are shown as small grey symbols. The triangles with error bars show the median and the 10th and 90th percentiles for the observations. In order to compare directly with the observations, we assume that 74 per cent of the cold gas mass predicted by the models is hydrogen.

in the two models (see Section 2.1). The dotted line in the bottom panel of Fig. 3 shows the effect on the standard Bow06 model of using Monte Carlo trees with a minimum mass $10^{10}\,h^{-1}\,{\rm M}_\odot(1+z)^{-3}$ instead of N-body trees with a fixed mass resolution (shown by the solid black line). The effect of improving the halo mass resolution is larger at high redshifts.

4.3 Gas-to-luminosity ratios of galaxies

Fig. 4 shows the gas-to-luminosity ratio as a function of absolute magnitude in the B band at $z = 0$ for late-type galaxies (those with bulge-to-total luminosity in the B band, $B/T \leq 0.4$, in order to make a fair comparison with observations), for the original models and with the new SF laws.

The Bau05 model predicts gas-to-luminosity ratios in good agreement with the observations, as these data were used as the main constraint on the parameters in the original SF recipe (equation 3). The new SF laws in the Bau05 model predict gas-to-luminosity ratios which increase with luminosity, contrary to the observed tendency. This is due to the new SF laws predicting generally shorter quiescent SF time-scales in low- and intermediate-mass galaxies but longer time-scales in high-mass galaxies, when compared to the original model (see Appendix C).

The original Bow06 model predicts gas-to-luminosity ratios which are in poor agreement with the observations, except at the highest luminosities. However, the new SF laws generally predict lower gas-to-luminosity ratios for galaxies fainter than $M_B - 5\log(h) \approx -20$, due to shorter quiescent SF time-scales, bringing them into better agreement with the observations.

5 THE EVOLUTION OF GALAXIES IN THE SFR VERSUS STELLAR MASS PLANE

The level of SF activity in galaxies at any redshift is dependent on the available cold gas and the time-scale on which the gas is consumed (which is set by the choice of SF law). Here we examine the influence of different SF laws on the distribution of galaxies in the SFR–stellar mass (SFR–$M_\star$) plane and its evolution with redshift. The distribution of galaxies in this plane offers a way to constrain the form of the SF law.

Brinchmann et al. (2004) found that local star-forming galaxies lie on a relatively narrow region in the SFR–$M_\star$ plane. Noeske et al. (2007), Elbaz et al. (2007) and Daddi et al. (2007) extended this work to higher redshifts, finding that the 'main sequence' of star-forming galaxies in the SFR–$M_\star$ plane remains in place up to at least $z \sim 2$ with a similar slope to that at $z \sim 0$. The zero-point evolves strongly with redshift. Santini et al. (2009) found evidence for a bimodal distribution of galaxies in the SFR–$M_\star$ plane, with a 'passive' sequence below that of actively star-forming galaxies. Below, we investigate whether or not the models are able to explain the observations, and to what extent the distribution of galaxies in the SFR–$M_\star$ constrains the SF law.

5.1 The local star formation rate–stellar mass plane

Fig. 5 shows the predicted distribution of galaxies in the SFR–$M_\star$ plane at $z = 0$ for the Bau05 and Bow06 models and for variants using the new SF laws. The colour shading indicates the regions within which 40 to 99 per cent of the model galaxies fall in the SFR–$M_\star$ plane, when the distributions are volume-weighted and normalized in bins of stellar mass. We also show, using solid and dotted black contours, the regions of the plane where satellite and burst galaxies respectively constitute more than 50 per cent of the population within cells in the SFR–$M_\star$ plane. Here we define burst galaxies as those in which the SB mode accounts for at least 20 per cent of their total SFR. Most of the galaxies (>99 per cent when integrated over the whole SFR–$M_\star$ plane) are undergoing quiescent SF. Some of these contours breakup into 'islands', but this is an artefact of some cells in the SFR–$M_\star$ plane containing a small number of galaxies.

We see from Fig. 5 that all of the models apart from the Bow06 model show two sequences in the SFR–$M_\star$ plane, although the shapes and widths of these sequences vary significantly depending on the SF law. We will call the upper sequence with higher SFRs at a given $M_\star$ the 'active' or 'star-forming' sequence, and the lower sequence with lower SFRs the 'passive' sequence. In the original Bow06 model there appears to be only an active sequence, but there is a large spread of galaxies down to lower SFRs. The two sequences appear more distinct for the variants of the Bow06 model with the new SF laws than for the Bau05 model and its variants. For the Bow06 model and variants, the active SF sequence extends down to the lowest stellar masses plotted, while for the Bau05 model and its variants the active sequence is only present for higher stellar masses. We now examine these differences in more detail.

In the Bau05 model and its variants, there are comparable numbers of active and passive galaxies for $M_\star \gtrsim 10^{10}\,h^{-1}\,\mathrm{M}_\odot$. At lower

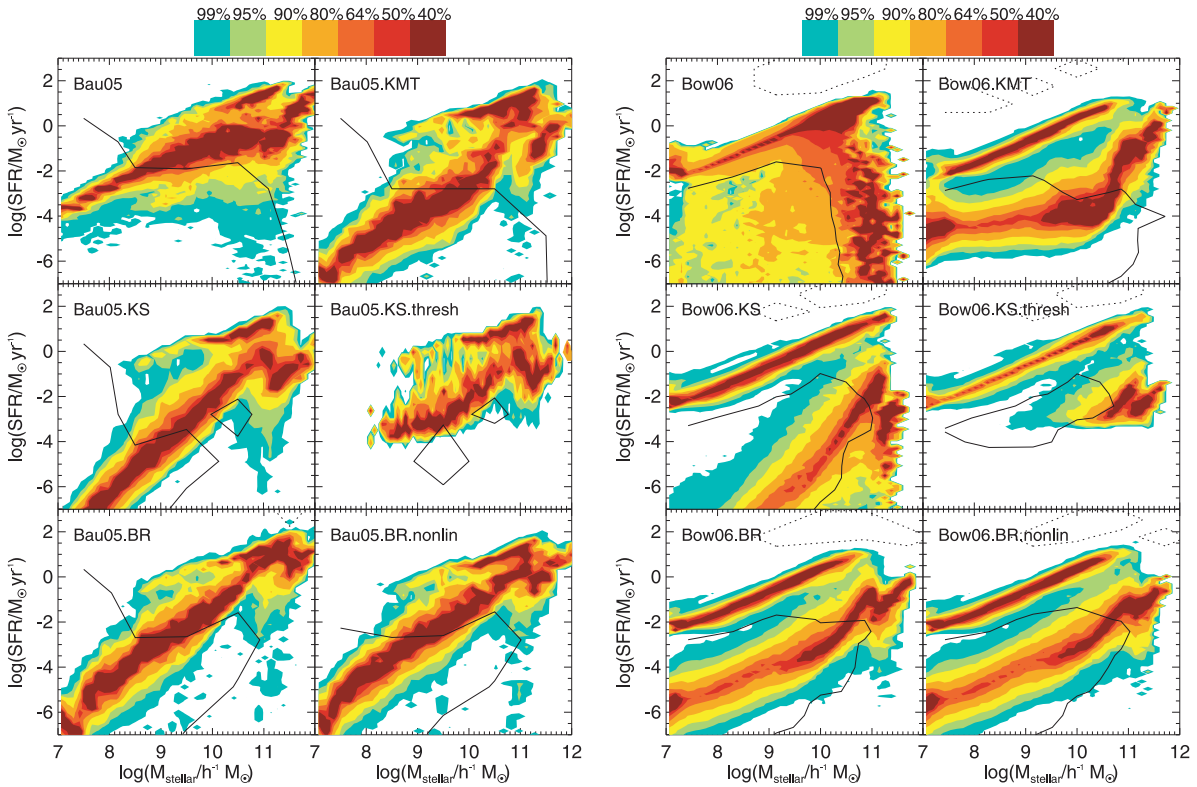

Figure 5. Distribution of galaxies in the SFR versus stellar mass plane at $z = 0$ for the Bau05 and the Bow06 models and their variants with the new SF laws (left- and right-hand sets of panels, respectively). Each panel corresponds to a different model, as labelled. The coloured contours show the regions within which different fractions of the galaxies lie for given stellar mass, volume-weighted and normalized in bins of stellar mass, with the scale shown by the key. We show, using dotted and solid black contours, the regions in which SB and satellite galaxies respectively make up more than 50 per cent of the galaxy population.

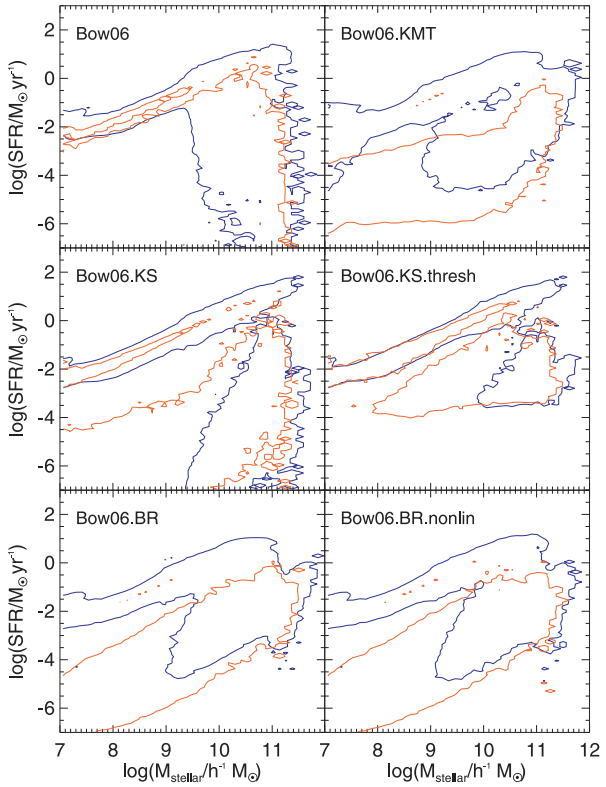

Figure 6. SFR versus stellar mass plane for galaxies at $z = 0$ in the Bow06 model with the different SF laws tested. The contours outline the 95 per cent percentile regions for satellite (red) and central (blue) galaxies, after normalizing in bins of stellar mass.

masses most of the galaxies are on the passive sequence, with the active sequence completely disappearing for $M_\star \lesssim 10^9\,h^{-1}\,\mathrm{M}_\odot$. The passive sequence is generally broader than the active one. The slope of the passive sequence is generally steeper with the new SF laws, producing lower SFRs at $M_\star \lesssim 10^{10}\,h^{-1}\,\mathrm{M}_\odot$. This is closely related to the lower gas content in these galaxies, as seen in Fig. 4. The exception is the KS.thresh law, where the passive sequence disappears at low SFR and low $M_\star$. This results from the cut-off in SF for galaxies with gas surface densities below the critical density (see equation 5). Indeed, 70 per cent of all galaxies in this model with $M_\star > 10^7\,h^{-1}\,\mathrm{M}_\odot$ have SFR = 0. However, in galaxies with $M_\star > 10^9\,h^{-1}\,\mathrm{M}_\odot$, this percentage falls to 30 per cent. This means that the critical density cut-off completely switches off SF activity in most low-mass galaxies at $z = 0$.

For the variants of the Bow06 model, the passive sequence appears generally narrower and more offset from the active one, compared to the Bau05 model variants; furthermore, there seems to be more dependence of the shape on the SF law. As for the Bau05.KS.thresh model, the passive sequence disappears completely at low SFRs in the Bow06.KS.thresh model.

In order to gain further insight into the nature of the upper and lower sequences in the SFR–$M_\star$ plane, we split the sample into central and satellite galaxies. Fig. 6 shows the 95 per cent percentile contours after normalization in bins of stellar mass, for central (blue contours) and satellite galaxies (red contours) for the Bow06 model and its variants. Satellite galaxies are found predominantly on the lower sequence, while the upper sequence is dominated by central galaxies, as expected from the solid black contours in Fig. 5. This implies that the inflow of newly cooled gas on to central galaxies is a key process in shaping the 'active' sequence, while the rate at which the cold gas reservoirs in satellite galaxies are consumed shapes the lower, 'passive' sequence. In satellite galaxies, the new SF laws applied to the Bow06 model typically produce longer SF time-scales (see Appendix C). This is a consequence of the new SF laws being non-linear in cold gas mass; hence, the SF time-scale becomes long when the gas mass becomes small, which happens when galaxies no longer accrete newly cooled gas. Therefore, satellite galaxies consume their gas reservoirs more slowly than in the original model, which results in larger cold gas masses and higher SFRs at later epochs, and allows the galaxies to remain on a well-defined sequence for longer. In contrast, with the old SF recipe the gas reservoirs of satellites decline exponentially with time.

The change in the slope of the passive sequence at $M_\star \sim 10^{10}\,h^{-1}\,\mathrm{M}_\odot$ in the Bow06.BR, Bow06.BR.nonlin and Bow06.KMT models is due to the change in the dominant regime in the $\Sigma_{\rm SFR}$–$\Sigma_{\rm gas}$ relation. Low-mass galaxies are predominantly in the low $\Sigma_{\rm gas}$ regime, for which most of the hydrogen is in the atomic phase, and the SFR has a steep dependence on $\Sigma_{\rm gas}$. Indeed, the steeper the relation in the $\Sigma_{\rm SFR}$–$\Sigma_{\rm gas}$ plane at low $\Sigma_{\rm gas}$, the flatter the passive sequence at low stellar masses (see Fig. 5 for the KMT SF law). However, this simple picture only holds for satellite galaxies, since central galaxies have a constant supply of newly cooled gas which shapes the upper sequence in the SFR–$M_\star$ plane, making it insensitive to the exact choice of SF law.

In the Bau05 model the satellite and central galaxy sequences overlap more due to the longer time-scale for gas to be reincorporated into the host halo after ejection by SNe, compared with the Bow06 model (see Section 2). This is particularly important at low stellar masses, for which SNe feedback is very efficient at ejecting gas which has previously cooled. The long reincorporation time-scale means that SF is nearly shut down in most low-mass central galaxies. Hence, the active SF sequence disappears at low $M_\star$. The passive sequence at low $M_\star$ therefore includes both satellite and central galaxies. We confirmed this by carrying out the exercise of applying the Bow06 prescription for the gas reincorporation time-scale in the Bau05 model, and found an active sequence which looks similar to that in the Bow06 model. The slope and dispersion of the active SF sequence are insensitive to the details of the SNe feedback (or the SF law; see Fig. 5), since making feedback stronger or weaker does not change its shape. We conclude that the reincorporation time-scale of the ejected gas is the main process controlling the form of the active SF sequence, while the passive sequence is mostly dependent on the choice of SF law. This relation offers a new way to constrain the SF law.

5.2 Comparison with observations of the SFR–$M_\star$ plane at $z = 0$

Indications of multiple sequences in the SFR–$M_\star$ plane have been found in the local Universe by Brinchmann et al. (2004), and at high redshifts by Damen et al. (2009), Santini et al. (2009) and Rodighiero et al. (2010). However, all of these studies are affected to some extent by selection effects against the inclusion of galaxies with low SFRs and/or low stellar masses, and these must be accounted for in any comparison with models. We start by comparing with observations of local galaxies in this subsection, and then consider higher redshifts in the next subsection.

In the top panel of Fig. 7 we show the observed distribution of galaxies in the SFR–$M_\star$ plane based on the Sloan Digital Sky

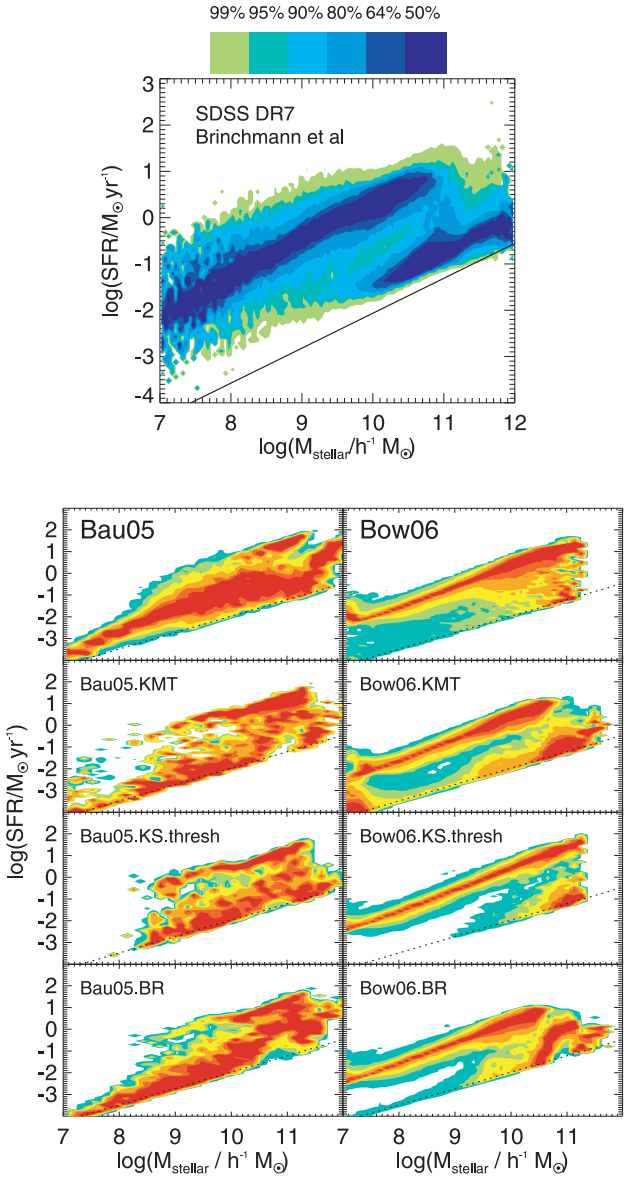

Figure 7. Top panel: observed distribution of galaxies in the SFR versus stellar mass plane for the SDSS DR7 spectroscopic sample of galaxies, updating the analysis by Brinchmann et al. (2004). The distributions are volume-weighted and normalized in bins of stellar mass as in Fig. 5, and the shading shows the regions within which different fractions of galaxies lie at each stellar mass. The black line shows the effective SFR sensitivity, which depends on stellar mass (Brinchmann, private communication). Bottom panel: the same as the top panel for model galaxies at $z = 0.1$ after applying the cuts used by Brinchmann et al. (2004) in the SDSS DR7 sample, for different models as labelled in each panel. For reference, the dotted lines show the sensitivity limit of the SFR estimates in the SDSS DR7. The shading is as in the top panel. The KS and BR.nonlin models are not shown due to their similarity with the KS.thresh and BR models, respectively.

Survey Data Release 7 (SDSS DR7),[4] which corresponds to an update of the Brinchmann et al. (2004) analysis. Stellar masses are determined from spectra and broad-band magnitudes following Kauffmann et al. (2003), while SFRs are derived primarily from

[4] Data were downloaded from the public webpage http://www.mpa-garching.mpg.de/SDSS/DR7/.

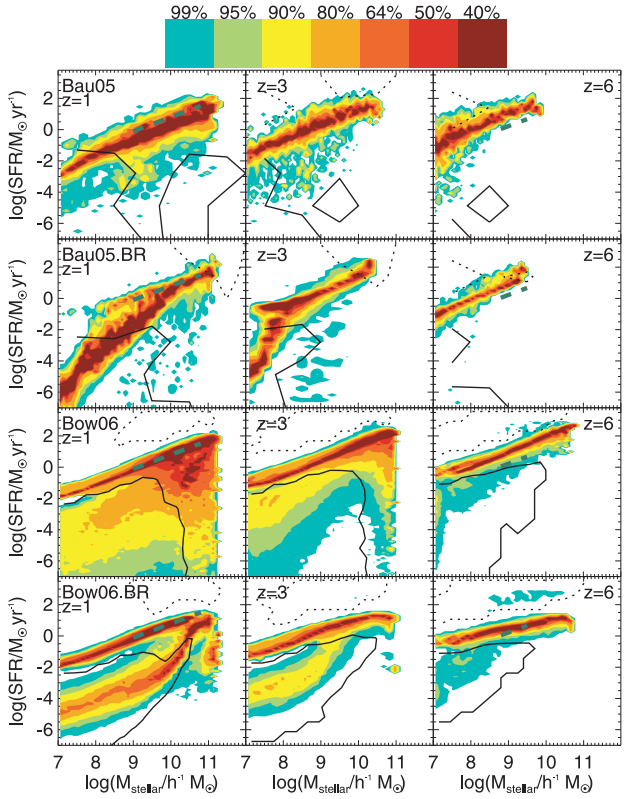

Figure 8. Distribution of galaxies in the SFR versus stellar mass plane at $z = 1$ (left column), $z = 3$ (middle column) and $z = 6$ (right column) for the Bau05 (top panel), the Bau05.BR (second panel), the Bow06 (third panel) and the Bow06.BR models (bottom panel). The shading shows the distribution of galaxies in this plane, normalized in bins of stellar mass. The thick dashed straight lines show the observations of the 'SF sequences' reported by Elbaz et al. (2007) at $z \sim 1$ and Stark et al. (2009) at $z \sim 6$, and are plotted over the mass ranges probed by the observations. We also show regions in which SB and satellite galaxies make up more than 50 per cent of the population using dotted and solid black contours, respectively.

the Hα emission line following Brinchmann et al. (2004). We refer the reader to these papers for further details. We have constructed contours of the distribution for the subsample of galaxies in the spectroscopic catalogue which have estimated SFRs, after volume-weighting and normalizing in bins of stellar mass. As in Fig. 5, the colour shading indicates the regions within which different fractions of galaxies lie for a given stellar mass. The solid black line shows the approximate SFR sensitivity limit in the SDSS analysis (Brinchmann, private communication). The minimum measurable SFR depends on stellar mass both because it depends on detecting spectral features above the stellar continuum, and because galaxies of higher $M_\star$ in the SDSS sample tend to lie at larger distances. Since the SDSS estimates are based on a Chabrier (2003) IMF for the stellar masses, and a Kroupa (2001) IMF for the SFRs, we rescale the stellar masses in the SDSS sample by a factor of 0.89 and the SFRs by a factor of 1.1 (Bell et al. 2003) to correspond to the use of a Kennicutt (1983) IMF for quiescent SF in the models. (In the Bau05 model SBs form stars with a top-heavy IMF, but this only affects a small fraction of the galaxies in the SFR–$M_\star$ plots. SB galaxies are typically located above the colour contours at higher SFRs, see dotted lines in Figs 5 and 8.)

To make the comparison with the SDSS data simpler and fairer, we plot the model predictions in the SFR–$M_\star$ plane again in the bottom panel of Fig 7, but this time imposing some additional

selections to better match the SDSS sample. Since the median redshift of the SDSS spectroscopic sample is around $z = 0.1$, we create a sample of model galaxies for $z = 0.1$, and then apply the apparent magnitude limit $r < 17.77$ of the SDSS spectroscopic sample. We also apply the SFR sensitivity limit of the SDSS sample shown in the top panel of Fig. 7. Fig 7 shows the SFR–$M_\star$ plane for the Bau05 (left-hand panels) and the Bow06 (right-hand panels) models at $z = 0.1$ after applying these cuts. Note that we do not show the BR.nonlin and KS models, given their similarity to the BR and KS.thresh, respectively.

For the SDSS sample plotted in Fig. 7, we see that most galaxies in the mass range $10^7 < M_\star \lesssim 10^{10}\,h^{-1}\,\mathrm{M}_\odot$ lie on a single star-forming sequence. At high masses $M_\star \gtrsim 10^{10}\,h^{-1}\,\mathrm{M}_\odot$, a second sequence appears, roughly parallel to the first but offset below it. Comparing with the model distributions in Fig. 7, the general distribution of galaxies in the SFR–$M_\star$ plane seems better matched by the variants of the Bow06 model rather than by any of the variants of the Bau05 model. All of the variants of the Bow06 model produce an upper star-forming sequence covering the whole mass range $10^7 < M_\star \lesssim 10^{11}\,h^{-1}\,\mathrm{M}_\odot$, with similar slope to the observed one, though with a smaller dispersion, particularly at low masses. The original Bow06 model does not reproduce the second sequence seen in the SDSS at high masses, but most of the variants with new SF laws do produce a similar feature. On the other hand, in the Bau05 model, the distribution of galaxies in the SFR–$M_\star$ plane appears rather different from the observed one. All the variants show an upper sequence of star-forming galaxies, which has a similar slope and amplitude to that seen in SDSS. However, this does not extend to low masses, unlike in the SDSS. The most prominent feature for the Bau05 model and its variants is the broad 'passive' sequence lying below the 'active' star-forming sequence, and extending down to the lowest masses plotted. This does not correspond to what is seen in the SDSS sample, where all low-mass galaxies appear to lie close to the 'active' star-forming sequence. The main origin of these differences between the Bau05 and Bow06 model for low stellar masses is the difference in the time-scale for the reincorporation into haloes of gas which has been ejected by SNe (see Section 6.1).

The passive sequence seen in Fig. 5 for the variants of the Bow06 model falls below the SFR sensitivity limit of the SDSS study at lower masses, $M_\star \lesssim 10^{10}\,h^{-1}\,\mathrm{M}_\odot$. However, observational indications of a passive galaxy sequence at low masses have been reported by Woo, Courteau & Dekel (2008) for Local Group dwarf galaxies. These objects follow a distinct SF sequence with much lower SFRs than the main star-forming sequence seen in the SDSS sample, similar to our predictions for passive galaxies in the Bow06 model variants with the new SF laws. Similarly, Skillman, Côté & Miller (2003) reported SFRs and stellar masses for galaxies in the Coma cluster which agree with the lower sequence seen in the top panel of Fig. 7, and also overlap with our prediction for massive satellite galaxies in the Bow06.BR, Bow06.BR.nonlin and Bow06.KMT models (Fig. 6).

5.3 The SFR–$M_\star$ relation at high redshift

Evidence for a star-forming sequence in the SFR–$M_\star$ plane has also been found at high redshifts. The slope of the observed relation seems to be constant over the redshift range probed, while the zero-point evolves strongly from $z \approx 0$ to $\sim$4 (Daddi et al. 2007; Elbaz et al. 2007; Pérez-González et al. 2008), but appears roughly constant for $4 \lesssim z \lesssim 6$ (Stark et al. 2009). However, we caution that the selection effects in some of the high-redshift samples are very strong, since some are selected on the basis of SFRs. Furthermore, the observational estimates of SFR and stellar mass typically become more uncertain at higher z, due to the more limited data available and the effects of dust (Stringer et al. 2011).

Both models in all of their variants predict an active SF sequence in good agreement with observations. The features of the models in the SFR–$M_\star$ plane at $z = 0$ (see Fig. 5) are preserved up to $z \approx 2$. At $z > 2$, the passive sequence starts to disappear, implying that at higher redshifts most of the galaxy population is undergoing vigorous SF and lies on the active SF sequence. To illustrate this general behaviour, Fig. 8 shows the predicted distribution of galaxies in the SFR–$M_\star$ plane at three different redshifts for the Bau05 and the Bow06 models, together with the BR variant. Also shown are the medians of the observed relations at different redshifts, plotted as thick dashed lines.[5]

Santini et al. (2009) found that bimodality in the SFR–$M_\star$ plane is clearly present in massive galaxies at $z \lesssim 1$, but becomes weaker as redshift increases, being almost absent at $z \sim 2$. This appears consistent with the predictions of the Bow06 model with the new SF laws, but is probably less so with predictions from the Bau05 model. However, the SFR sensitivity limit in the sample of Santini et al. is quite high (SFR $\gtrsim 10^{-2}\,\mathrm{M}_\odot\,\mathrm{yr}^{-1}$) relative to the model predictions at lower masses, making it difficult to study the passive population at high redshift.

The new SF laws, through their impact on the cold gas contents of galaxies, strongly affect the passive population and its evolution as seen in the SFR–$M_\star$ plane, in a way that could be used as an important constraint on the SF model, if observational data could probe low enough SFRs. On the other hand, the active SF sequence is much less affected by the choice of SF law, but instead depends on the assumption about how quickly gas ejected by SN feedback is reincorporated into the host halo.

6 DISCUSSION AND CONCLUSIONS

Improvements in the quality and quantity of observations of the spatially resolved SFRs and atomic and molecular gas contents in local galaxies (e.g. Kennicutt et al. 2007; Bigiel et al. 2008) have allowed the development of both empirical (e.g. BR06; Leroy et al. 2008) and theoretical SF models (Krumholz et al. 2009b). These models prescribe a relation between the surface density of SF $\Sigma_{\rm SFR}$ and gas $\Sigma_{\rm gas}$, often depending also on other physical quantities such as the stellar surface density and gas metallicity. We have revisited the SF recipes for quiescent galaxy formation in galaxy discs used in the galaxy formation model GALFORM and implement new, parameter-free SF laws with the aim of isolating observations that could be used to distinguish between SF models (see Lagos et al. 2011, for the predictions of these models for the atomic and molecular hydrogen content of galaxies).

We test the following SF laws: (i) the Schmidt law, which has the form $\Sigma_{\rm SFR} \propto \Sigma_{\rm gas}^N$ with $N = 1.4$ (the KS law) and (ii) its variant, the Kennicutt–Schmidt law, which includes an SF cut-off at low gas surface densities, motivated by gravitational stability considerations (Toomre 1964; the KS.thresh law); (iii) an SF law of the form $\Sigma_{\rm SFR} \propto \nu_{\rm SF} f_{\rm mol}\,\Sigma_{\rm gas}$, where $f_{\rm mol}$ depends on the hydrostatic gas pressure (see equation 7; BR06; Leroy et al. 2008), and $\nu_{\rm SF}$ is an inverse time-scale of SF activity in molecular gas, assumed to

[5] Since in the observational samples a universal Salpeter IMF was assumed when estimating SFRs and stellar masses, we scale their stellar masses and SFRs by factors of 0.5 and 0.91, respectively (e.g. Bell et al. 2003), to correspond to a Kennicutt (1983) IMF.

be constant (the BR law); (iv) a variant of the previous SF law, but assuming $\nu_{\rm SF} = \nu_{\rm SF}(\Sigma_{\rm gas})$ which depends on the total gas surface density (see equation 9; the BR.nonlin law) and (v) the theoretical SF law of Krumholz et al. (2009b) in which the ratio of surface densities of molecular to atomic gas depends on the balance between the dissociation of molecules due to the interstellar far-UV radiation and their formation on the surface of dust grains (the KMT law). We apply the new SF laws to the quiescent SF mode which takes place in galactic discs (see Section 2.1).

We have applied the new SF laws to two variants of GALFORM, those of Bau05 and Bow06. These models have many differences in their input physics, including different laws for quiescent SF, and furthermore their parameters were tuned to reproduce different sets of observational constraints. We have left the parameters for all other physical processes, including SF in SBs and feedback from SNe and AGN, unchanged when running with the new quiescent SF laws, rather than retuning these other parameters to try to reproduce the original observational constraints. This allows us to isolate the impact of invoking different SF laws. Previous attempts to include similar SF recipes in semi-analytical models have not focused on how galaxy properties are affected by changing the SF law alone, but have also made changes to other model parameters (e.g. Cook et al. 2010; Dutton et al. 2010; Fu et al. 2010).

The choice of quiescent SF law by construction affects the quiescent SF activity. In the most extreme case, the cosmic SFR density in the quiescent mode changes by an order of magnitude when compared with the original model. However, the total SFR density evolution is remarkably insensitive to the choice of SF law. In the case of the Bau05 model the new SF laws increase the SFR in the quiescent mode, while the contrary happens in the Bow06 model. This is compensated for by weaker SB activity in the Bau05 model and more vigorous SBs in the Bow06 model. This adjustment is particularly effective in the case of the Bow06 model, which includes SBs triggered by disc instabilities. A related consequence is the insensitivity of the present-day $b_{\rm J}$-band LF and $g - r$ colour distributions and the evolution of the K-band LF to the choice of quiescent SF law.

Since the gas is consumed at different rates during quiescent and SB SF, the change in the quiescent SF law leads to large differences in the cold gas content of galaxies. For both models the new SF laws predict more galaxies with low cold gas masses, fewer with intermediate cold gas masses and similar or fewer with high cold masses. This leads to a lower cosmic mean cold gas density at all redshifts. For the Bow06 model, these changes help to improve the agreement with the local observations by Zwaan et al. (2005). We find similar changes in the $M_{\rm H}/L_B$ gas-to-light ratios as functions of luminosity.

Finally, we investigated the distribution of galaxies in the SFR–$M_\star$ plane at different redshifts for both the old and new SF laws. In most cases, the models predict two sequences in this plane, an 'active' sequence with higher SFRs and a 'passive' sequence with lower SFRs. The form of the 'active' sequence, which is dominated by central galaxies, appears insensitive to the quiescent SF law. This can be understood in terms of a rough balance being set up between accretion of gas due to cooling in the halo and consumption of gas by SF and ejection by SN feedback (at a rate which is proportional to the SFR). The cold gas mass in a galaxy therefore adjusts to achieve this balance (for a given SF law), while the SFR itself is insensitive to the SF law. The form of the active sequence is, however, sensitive to the time-scale for gas which has been ejected by SN feedback to be reincorporated into the halo, particularly in low-mass galaxies where the SN feedback is very effective at ejecting gas. This reincorporation time-scale is relatively short (around a halo dynamical time) in the Bow06 model, but longer in the Bau05 model. As a consequence, the active sequence extends down to very low stellar masses in the Bow06 model and its variants with different SF laws, but it disappears at low masses in the Bau05 model and its variants.

The form of the 'passive' sequence, where most satellite galaxies are found, is much more sensitive to the SF law. Satellite galaxies are assumed to not accrete any cold gas; thus, they are simply using up existing reservoirs of cold gas by SF and feedback, and their gas contents and SFRs are thus sensitive to the rate at which this has happened over their history. This depends on the SF law and weakly on other parameters, such as SN feedback. We propose that the direct measurement of the (low) SFR of passive galaxies offers a constraint on the SF law and can be directly compared with the predictions made in this work.

We made a qualitative comparison of the predicted distribution of galaxies in the SFR–$M_\star$ plane with observational data. For $z \approx 0$, we compared with the SDSS DR7 results of Brinchmann et al. (2004) which show two sequences, of active and passive galaxies, at high stellar masses. The Bow06 model variants (particularly those with the BR, BR.nonlin or the KMT SF laws) appear in better agreement with these data than the Bau05 model, after accounting for the sensitivity limits. Observations at higher redshifts indicate the presence of an active SF sequence that evolves in normalization but not in slope (e.g. Brinchmann et al. 2004; Daddi et al. 2007; Elbaz et al. 2007; Stark et al. 2009). The model predictions appear in general agreement with these observations for both the Bau05 and Bow06 models and their variants. Rodighiero et al. (2010) and Santini et al. (2009) have found indications of bimodality at $z \sim 1$ in massive galaxies, consistent with our predictions for the Bow06 model in the three variants already mentioned.

Future observations of SFRs, stellar masses and particularly the gas contents of galaxies at high redshifts will be crucial for testing whether current ideas about SF laws applied at earlier stages in galaxy evolution. Telescopes such as ALMA, *James Webb Space Telescope* and extremely large telescopes will make possible measurements of very low SFRs such as those predicted here for the passive galaxy population, while observations with ALMA, ASKAP, MeerKAT and eventually SKA will be critical for measuring the molecular and atomic gas contents of high-redshift galaxies. In this way we will be able to confirm or rule out the predictions of the models presented here.

ACKNOWLEDGMENTS

We thank Shaun Cole, Mark Swinbank, Martin Stringer, Jarle Brinchmann, Dave Gilbank and Violeta González for useful comments and discussions. We thank the anonymous referee for helpful remarks that enable us to improve the presentation of this work. CPL gratefully acknowledges an STFC Gemini studentship. AJB acknowledges the support of the Gordon & Betty Moore Foundation. This work was supported by a rolling grant from the STFC.

REFERENCES

Almeida C., Baugh C. M., Lacey C. G., 2007, MNRAS, 376, 1711
Baugh C. M., 2006, Rep. Progress Phys., 69, 3101
Baugh C. M. et al., 2004, MNRAS, 351, L44
Baugh C. M., Lacey C. G., Frenk C. S., Granato G. L., Silva L., Bressan A., Benson A. J., Cole S., 2005, MNRAS, 356, 1191 (Bau05)
Bell E. F., Baugh C. M., Cole S., Frenk C. S., Lacey C. G., 2003, MNRAS, 343, 367

Benson A. J., 2010, Phys. Rep., 495, 33
Benson A. J., Bower R., 2010, MNRAS, 405, 1573
Benson A. J., Bower R. G., Frenk C. S., Lacey C. G., Baugh C. M., Cole S., 2003, ApJ, 599, 38
Bigiel F., Leroy A., Walter F., Brinks E., de Blok W. J. G., Madore B., Thornley M. D., 2008, AJ, 136, 2846
Blitz L., Rosolowsky E., 2006, ApJ, 650, 933 (BR06)
Booth R. S., de Blok W. J. G., Jonas J. L., Fanaroff B., 2009, preprint (arXiv:0910.2935)
Bouché N. et al., 2007, ApJ, 671, 303
Bower R. G., Benson A. J., Malbon R., Helly J. C., Frenk C. S., Baugh C. M., Cole S., Lacey C. G., 2006, MNRAS, 370, 645 (Bow06)
Bower R. G., Vernon I., Goldstein M., Benson A. J., Lacey C. G., Baugh C. M., Cole S., Frenk C. S., 2010, MNRAS, 407, 2017
Brinchmann J., Charlot S., White S. D. M., Tremonti C., Kauffmann G., Heckman T., Brinkmann J., 2004, MNRAS, 351, 1151
Bromm V., Larson R. B., 2004, ARA&A, 42, 79
Calzetti D. et al., 2007, ApJ, 666, 870
Caputi K. I., McLure R. J., Dunlop J. S., Cirasuolo M., Schael A. M., 2006, MNRAS, 366, 609
Cattaneo A., Dekel A., Faber S. M., Guiderdoni B., 2008, MNRAS, 389, 567
Chabrier G., 2003, PASP, 115, 763
Cole S., Aragon-Salamanca A., Frenk C. S., Navarro J. F., Zepf S. E., 1994, MNRAS, 271, 781
Cole S., Lacey C. G., Baugh C. M., Frenk C. S., 2000, MNRAS, 319, 168
Cole S. et al., 2001, MNRAS, 326, 255
Cook M., Evoli C., Barausse E., Granato G. L., Lapi A., 2010, MNRAS, 402, 941
Cora S. A., 2006, MNRAS, 368, 1540
Daddi E. et al., 2007, ApJ, 670, 156
Damen M., Labbé I., Franx M., van Dokkum P. G., Taylor E. N., Gawiser E. J., 2009, ApJ, 690, 937
Drory N., Bender R., Feulner G., Hopp U., Maraston C., Snigula J., Hill G. J., 2004, ApJ, 608, 742
Dutton A. A., van den Bosch F. C., Dekel A., 2010, MNRAS, 405, 1690
Dutton A. A. et al., 2011, MNRAS, 410, 1660
Elbaz D. et al., 2007, A&A, 468, 33
Elmegreen B. G., 1993, ApJ, 411, 170
Fanidakis N., Baugh C. M., Benson A. J., Bower R. G., Cole S., Done C., Frenk C. S., 2011, MNRAS, 410, 58
Fu J., Guo Q., Kauffmann G., Krumholz M. R., 2010, MNRAS, 409, 515
Fumagalli M., Gavazzi G., 2008, A&A, 490, 571
Fumagalli M., Krumholz M. R., Hunt L. K., 2010, ApJ, 722, 919
Genzel R. et al., 2010, MNRAS, 407, 2091
Gil de Paz A. et al., 2007, ApJS, 173, 185
González J. E., Lacey C. G., Baugh C. M., Frenk C. S., Benson A. J., 2009, MNRAS, 397, 1254
González J. E., Lacey C. G., Baugh C. M., Frenk C. S., 2011, MNRAS, 413, 749
Gonzalez-Perez V., Baugh C. M., Lacey C. G., Almeida C., 2009, MNRAS, 398, 497
Hartwick F. D. A., 1971, ApJ, 163, 431
Helfer T. T., Thornley M. D., Regan M. W., Wong T., Sheth K., Vogel S. N., Blitz L., Bock D., 2003, ApJS, 145, 259
Heyer M. H., Corbelli E., Schneider S. E., Young J. S., 2004, ApJ, 602, 723
Huchtmeier W. K., Richter O., 1988, A&A, 203, 237
Johnston S. et al., 2008, Exp. Astron., 22, 151
Kauffmann G., Charlot S., 1998, MNRAS, 294, 705
Kauffmann G. et al., 2003, MNRAS, 341, 54
Kennicutt R. C., Jr, 1983, ApJ, 272, 54
Kennicutt R. C., Jr, 1989, ApJ, 344, 685
Kennicutt R. C., Jr, 1998, ApJ, 498, 541 (K98)
Kennicutt R. C., Jr, et al., 2007, ApJ, 671, 333
Kim H., Baugh C. M., Benson A. J., Cole S., Frenk C. S., Lacey C. G., Power C., Schneider M., 2011, MNRAS, 414, 2367
Kochanek C. S. et al., 2001, ApJ, 560, 566
Kregel M., van der Kruit P. C., de Grijs R., 2002, MNRAS, 334, 646
Kroupa P., 2001, MNRAS, 322, 231
Krumholz M. R., McKee C. F., 2005, ApJ, 630, 250
Krumholz M. R., Tan J. C., 2007, ApJ, 654, 304
Krumholz M. R., McKee C. F., Tumlinson J., 2009a, ApJ, 693, 216
Krumholz M. R., McKee C. F., Tumlinson J., 2009b, ApJ, 699, 850
Lacey C., Guiderdoni B., Rocca-Volmerange B., Silk J., 1993, ApJ, 402, 15
Lacey C. G., Baugh C. M., Frenk C. S., Silva L., Granato G. L., Bressan A., 2008, MNRAS, 385, 1155
Lacey C. G., Baugh C. M., Frenk C. S., Benson A. J., Orsi A., Silva L., Granato G. L., Bressan A., 2010, MNRAS, 405, 2
Lacey C. G., Baugh C. M., Frenk C. S., Benson A. J., 2011, MNRAS, 412, 1828
Lagos C. D. P., Cora S. A., Padilla N. D., 2008, MNRAS, 388, 587
Lagos C. d. P., Baugh C. M., Lacey C. G., Benson A. J., Power C., Kim H., 2011, MNRAS, submitted, preprint (arXiv:1105.2294)
Le Delliou M., Lacey C. G., Baugh C. M., Morris S. L., 2006, MNRAS, 365, 712
Leroy A. K., Walter F., Brinks E., Bigiel F., de Blok W. J. G., Madore B., Thornley M. D., 2008, AJ, 136, 2782
Leroy A. K. et al., 2009, AJ, 137, 4670
McKee C. F., Krumholz M. R., 2010, ApJ, 709, 308
McKee C. F., Ostriker E. C., 2007, ARA&A, 45, 565
Madore B. F., 1977, MNRAS, 178, 1
Martin C. L., Kennicutt R. C., Jr, 2001, ApJ, 555, 301
Mo H. J., Mao S., White S. D. M., 1998, MNRAS, 295, 319
Monaco P., Fontanot F., Taffoni G., 2007, MNRAS, 375, 1189
Noeske K. G. et al., 2007, ApJ, 660, L43
Norberg P. et al., 2002, MNRAS, 336, 907
Onodera S. et al., 2010, ApJ, 722, L127
Orsi A., Lacey C. G., Baugh C. M., Infante L., 2008, MNRAS, 391, 1589
Parkinson H., Cole S., Helly J., 2008, MNRAS, 383, 557
Pérez-González P. G. et al., 2008, ApJ, 675, 234
Péroux C., McMahon R. G., Storrie-Lombardi L. J., Irwin M. J., 2003, MNRAS, 346, 1103
Power C., Baugh C. M., Lacey C. G., 2010, MNRAS, 406, 43
Pozzetti L. et al., 2003, A&A, 402, 837
Press W. H., Teukolsky S. A., Vetterling W. T., Flannery B. P., 1992, Numerical Recipes in FORTRAN. The Art of Scientific Computing, 2nd edn. Cambridge Univ. Press, Cambridge
Rao S., Briggs F., 1993, ApJ, 419, 515
Rodighiero G. et al., 2010, A&A, 518, L25
Rosolowsky E., Blitz L., 2005, ApJ, 623, 826
Roychowdhury S., Chengalur J. N., Begum A., Karachentsev I. D., 2009, MNRAS, 397, 1435
Sage L. J., 1993, A&AS, 100, 537
Sanduleak N., 1969, AJ, 74, 47
Santini P. et al., 2009, A&A, 504, 751
Saracco P. et al., 2006, MNRAS, 367, 349
Schaye J., 2004, ApJ, 609, 667
Schaye J. et al., 2010, MNRAS, 402, 1536
Schilizzi R. T., Dewdney P. E. F., Lazio T. J. W., 2008, in Stepp L., Gilmiozzi R., Hall H., eds, Proc. SPIE Conf. Ser. Vol. 7733, The Square Kilometre Array. SPIE, Bellingham, p. 18.
Schmidt M., 1959, ApJ, 129, 243
Schruba A., Leroy A. K., Walter F., Sandstrom K., Rosolowsky E., 2010, ApJ, 722, 1699
Schuster K. F., Kramer C., Hitschfeld M., Garcia-Burillo S., Mookerjea B., 2007, A&A, 461, 143
Shen S., Mo H. J., White S. D. M., Blanton M. R., Kauffmann G., Voges W., Brinkmann J., Csabai I., 2003, MNRAS, 343, 978
Shu F. H., 1973, in Greenberg J. M., van de Hulst H. C., eds, Proc. IAU Symp. 52, Interstellar Dust and Related Topics. Kluwer, Dordrecht, p. 257
Silk J., Norman C., 2009, ApJ, 700, 262
Skillman E. D., Côté S., Miller B. W., 2003, AJ, 125, 593
Solomon P. M., Sage L. J., 1988, ApJ, 334, 613
Solomon P. M., Vanden Bout P. A., 2005, ARA&A, 43, 677

Springel V., 2005, MNRAS, 364, 1105
Springel V., White S. D. M., Tormen G., Kauffmann G., 2001, MNRAS, 328, 726
Stark D. P., Ellis R. S., Bunker A., Bundy K., Targett T., Benson A., Lacy M., 2009, ApJ, 697, 1493
Stringer M. J., Benson A. J., 2007, MNRAS, 382, 641
Stringer M., Cole S., Frenk C. S., Stark D. P., 2011, MNRAS, 414, 1927
Tan J. C., 2000, ApJ, 536, 173
Toomre A., 1964, ApJ, 139, 1217
Walter F., Brinks E., de Blok W. J. G., Bigiel F., Kennicutt R. C., Thornley M. D., Leroy A., 2008, AJ, 136, 2563
White S. D. M., Frenk C. S., 1991, ApJ, 379, 52
Wong T., Blitz L., 2002, ApJ, 569, 157
Woo J., Courteau S., Dekel A., 2008, MNRAS, 390, 1453
Wyder T. K. et al., 2009, ApJ, 696, 1834
Zwaan M. A., Briggs F. H., Sprayberry D., Sorar E., 1997, ApJ, 490, 173
Zwaan M. A., Meyer M. J., Staveley-Smith L., Webster R. L., 2005, MNRAS, 359, L30

APPENDIX A: NUMERICAL INTEGRATION OF THE STAR FORMATION EQUATIONS

Here we outline the numerical solution of the equations that describe the changes in the baryonic content of galaxies, namely the hot gas, cold gas, stellar mass and the metals in each component.

A1 The instantaneous SFR

The radial profiles of galactic discs are not resolved in GALFORM (except in special cases, e.g. Stringer & Benson 2007). We assume discs are described by an exponential profile (see Cole et al. 2000),

$$\Sigma_{\rm disc}(R) = \Sigma_0 e^{-R/r_{\rm eff}}, \tag{A1}$$

where $r_{\rm eff}$ is the scalelength of the disc, $\Sigma_0 = M_{\rm disc}/2\pi r_{\rm eff}^2$ is the central surface density and $M_{\rm disc}$ is the disc mass in the component traced (i.e. the cold gas mass, $M_{\rm cold}$ for $\Sigma_{\rm gas}$, or the stellar mass of the disc, $M_{\rm stellar,disc}$ for $\Sigma_{\rm stellar}$). Note that $r_{\rm eff}$ in an exponential disc is related to the half-mass radius by $r_{50} = 1.67 r_{\rm eff}$.

The instantaneous SFR in a given episode will be the surface integral of $\Sigma_{\rm SFR}$ over the full disc, except for the case of the KS.thresh SF law, in which we integrate only over the unstable region, which corresponds to the solutions of $\Sigma_{\rm gas} = \Sigma_{\rm crit}$ (see equation 5). In the case that the integral cannot be solved analytically (as in the BR, BR.nonlin and KMT SF laws), we use Romberg integration to compute the global SFR by integrating $\Sigma_{\rm SFR}(R)$ over the whole disc. This method uses adaptive, equally spaced divisions in R to achieve the required accuracy in each calculation. For simplicity, we do not distribute the newly formed stars only over the part of the disc where the SF activity occurs, but instead we assume that gas and stars are always distributed with the same exponential profile. Stringer & Benson (2007) found this to be a reasonable approximation for the gas component in their radially resolved calculations of galactic disc evolution. However, this approximation could overestimate the radial extent of the stellar component of the disc in gas-dominated galaxies (see Stringer & Benson 2007; we revisit this point in Appendix C2).

A2 The SF equations

The SF activity in GALFORM is regulated by three channels: (i) accretion of gas which cools from hot gas haloes on to the disc, (ii) SF from the cold gas and (iii) reheating and ejection of gas due to SNe feedback. These channels modify the mass and metallicity of each of the mass components (i.e. stellar mass, $M_\star$, cold gas mass, $M_{\rm cold}$, hot halo gas mass, $M_{\rm hot}$, and their respective masses in metals, $M_\star^Z$, $M_{\rm cold}^Z$ and $M_{\rm hot}^Z$). The system of equations relating these quantities is (Cole et al. 2000)

$$\dot{M}_\star = (1-R)\psi \tag{A2}$$

$$\dot{M}_{\rm cold} = \dot{M}_{\rm cool} - (1-R+\beta)\psi \tag{A3}$$

$$\dot{M}_{\rm hot} = -\dot{M}_{\rm cool} + \beta\psi \tag{A4}$$

$$\dot{M}_\star^Z = (1-R) Z_{\rm cold}\psi \tag{A5}$$

$$\dot{M}_{\rm cold}^Z = \dot{M}_{\rm cool} Z_{\rm hot} + [p - (1+\beta-R) Z_{\rm cold}]\psi \tag{A6}$$

$$\dot{M}_{\rm hot}^Z = -\dot{M}_{\rm cool} Z_{\rm hot} + (p\,e + \beta Z_{\rm cold})\psi. \tag{A7}$$

Here p denotes the yield (the fraction of mass converted into stars that is returned to the ISM in the form of metals), e is the fraction of newly produced metals ejected directly from the stellar disc to the hot gas phase, R is the fraction of mass recycled to the ISM (in the form of stellar winds and SN explosions), $Z_{\rm cold} = M_{\rm cold}^Z/M_{\rm cold}$ is the metallicity of the cold gas and β is the efficiency of stellar feedback. Descriptions of the feedback mechanisms can be found in Benson et al. (2003) and Lacey et al. (2008). These equations are defined as a function of the instantaneous SFR, ψ, that in the standard version of GALFORM has the form given by equation (1), with $\psi \propto M_{\rm cold}$. This form of the SFR has the advantage that equations (15)–(20) can be solved analytically assuming that $\dot{M}_{\rm cool}$ is constant over a time-step.

The new SF laws are non-linear in $M_{\rm cold}$, so they require equations (A2)–(A7) to be solved numerically. Once ψ (Section 2.3.1) is calculated, we proceed to integrate equations (A2)– (A7). In GALFORM, the equations tracking the evolution of the baryons are integrated over 'halo time-steps' given by the time resolution at which the halo merger tree is stored, which in the case of both N-body and Monte Carlo trees is independent of the individual SF time-scales in each galaxy. Hence, for some cases, the halo time-step could be large compared to the SF time-scale. This makes it necessary to solve equations (A2)– (A7) using adaptive step sizes to achieve accurate solutions. We use the fourth-order Runge–Kutta (RK) method with adaptive step sizes (Press et al. 1992). The quantities involved in the calculation of the instantaneous SFR, such as stellar mass, gas mass and metallicity of the gas, are updated in each substep. However, for simplicity, we assume that the disc scalelength $r_{\rm eff}$ and $\dot{M}_{\rm cool}$ (see equation A1) remain constant during the integration over each halo step. After integrating equations (15)– (20), we infer the galaxy luminosity by integrating the SF history over a halo time-step, interpolating the SFR between the values output at the substeps of the RK integration.

APPENDIX B: THE STAR FORMATION LAWS

In this appendix we explain more extensively some physical details of the new SF laws included in the GALFORM model.

B1 The critical surface density of the K98 star formation law

In a thin isothermal disc, the critical surface density for gravitational instability of axisymmetric perturbations, $\Sigma_{\rm crit}$, is given by

$$\Sigma_{\rm crit} = \frac{\kappa\,\sigma_{\rm g}}{Q_{\rm crit}\,\pi G}, \tag{B1}$$

where $Q_{\rm crit}$ is a dimensionless constant $\sim$1 (Toomre 1964), $\sigma_{\rm g}$ is the velocity dispersion of the gas and κ is the epicyclic frequency of the disc. For realistic gas/stellar discs we expect $Q_{\rm crit} > 1$ due to the effects of non-axisymmetric instabilities and the gravity of the stars (see references in K89). It has been shown that $\sigma_{\rm g}$ is approximately constant within discs. This means that the radial dependence of $\Sigma_{\rm crit}$ is determined by that of κ, and can be estimated directly from a galaxy rotation curve,

$$\kappa = \sqrt{2}\frac{V}{R}\left(1 + \frac{R}{V}\frac{{\rm d}V}{{\rm d}R}\right)^{1/2}. \quad \text{(B2)}$$

For a flat rotation curve,

$$\Sigma_{\rm crit} = \frac{\sqrt{2}}{Q_{\rm crit}\,\pi G}\,\sigma_{\rm g}\,\frac{V}{R}. \quad \text{(B3)}$$

K89 compared $\Sigma_{\rm crit}$ with the gas profile of the disc ($\Sigma_{\rm gas}$), and found that at the radius of the outermost H II regions (which indicate recent SF activity), $\Sigma_{\rm gas}/\Sigma_{\rm crit} \approx 1.9$–$3.3$ for $Q_{\rm crit} = 1$ (after scaling by our choice of $\sigma_{\rm g}$). The median corresponds to $Q_{\rm crit} \approx 2.5$.

B2 The mid-plane hydrostatic pressure of disc galaxies

Under the assumptions of local isothermal stellar and gas layers, and $\sigma_\star > \sigma_{\rm g}$, the mid-plane hydrostatic pressure in discs, $P_{\rm ext}$, can be approximated to within 10 per cent by (Elmegreen 1993)

$$P_{\rm ext} \approx \frac{\pi}{2} G \Sigma_{\rm gas}\left[\Sigma_{\rm gas} + \left(\frac{\sigma_{\rm g}}{\sigma_\star}\right)\Sigma_\star\right], \quad \text{(B4)}$$

where $\Sigma_{\rm gas}$ and $\Sigma_\star$ are the total surface densities of gas and stars, respectively, and $\sigma_{\rm g}$ and $\sigma_\star$ give the vertical velocity dispersion of the gas and stars. We assume a constant gas velocity dispersion, $\sigma_{\rm g} = 10\,{\rm km\,s^{-1}}$ (see Section 2.2.1). By assuming that $\Sigma_\star \gg \Sigma_{\rm gas}$, $\sigma_\star = \sqrt{\pi G\, h_\star \Sigma_\star}$, where $h_\star$ is the stellar scaleheight. This approximation could break down for very high redshift galaxies, whose discs are gas dominated. In such cases, we assume a floor of $\sigma_\star \geq \sigma_{\rm g}$. We estimate the stellar scaleheight assuming that it is proportional to the radial scalelength of the disc, as observed in local spiral galaxies, with $r_{\rm eff}/h_\star \approx 7.3 \pm 1.2$ (Kregel, van der Kruit & de Grijs 2002).

B3 The KMT star formation law

KMT theoretical model attempts to deal with three problems: (i) the determination of the fraction of gas in the molecular phase; (ii) the estimation of the characteristic properties (masses and surface densities) of GMCs, using a mixture of theoretical ideas and observed correlations, and (iii) the estimation of the rate at which molecular clouds convert themselves into stars. The latter rate is known observationally to be very small ($\approx$1 per cent of mass per free-fall time; Krumholz & Tan 2007) and is understood as a result of the regulation of the SF activity by supersonic turbulence (Krumholz & McKee 2005). KMT09 write the SFR per unit total gas mass as a function of two factors, the fraction of gas in the molecular phase, $f_{\rm mol}$ (see previous subsection), and the SFR per unit molecular mass, $\nu_{\rm SF}$, as in equation (8).

B3.1 The molecular-to-total gas ratio

The fraction $f_{\rm mol}$ depends on metallicity and the gas surface density of the atomic–molecular complex. The KMT09 expression for the molecular-to-total gas fraction predicts that in very metal poor environments, $f_{\rm mol} \to 0$. If implemented at face value, this would prevent any SF from taking place in pristine gas at very high redshift, and consequently there would be no enrichment to make possible any subsequent SF. However, this behaviour results from neglecting gas-phase reactions for the formation of H_2 molecules, which dominate over formation on dust grains when the metallicity is very low. Guided by the results of calculations of the formation of the first stars (see Bromm & Larson 2004, for a review), we will therefore assume that a minimum $f_{\rm mol}^{\rm min} = 10^{-4}$ applies at the onset of the SF activity in our implementation.

B3.2 The star formation time-scale

KMT define the inverse of the time-scale needed to consume the gas in a cloud into stars as $\nu_{\rm SF} = \epsilon_{\rm ff}/t_{\rm ff}$, where $t_{\rm ff}$ is the free-fall time of a GMC and $\epsilon_{\rm ff}$ is the fraction of gas converted to stars per free-fall time (see Krumholz & McKee 2005). In this model, $\epsilon_{\rm ff}$ is a weak function of cloud properties, but the free-fall time $t_{\rm ff}$ depends on the cloud mass $M_{\rm cl}$ and surface density $\Sigma_{\rm cl}$. KMT assume that the GMC mass corresponds to the critical Jeans mass for gravitational instability, and that GMCs are embedded in a gaseous disc that is marginally stable by the Toomre (1964) condition ($Q = 1$). KMT09 then use an observed correlation found for nearby galaxies between the global angular velocity of rotation around a galaxy and the gas surface density, which leads to $M_{\rm cl} \propto \Sigma_{\rm gas}$.

APPENDIX C: AN ILLUSTRATION OF THE IMPACT OF APPLYING DIFFERENT STAR FORMATION LAWS

The semi-analytical model follows a range of physical processes, as set out in Section 2. The interplay between these makes it difficult to disentangle the impact of one ingredient in isolation. To gain an understanding of the consequences of changing the SF law, we take the outputs of the original Bau05 and Bow06 models, and calculate the SFR using the SF prescriptions in Section 2, and compare with the SFR in the original model. To do this, we freeze the physical properties of the galaxy used in the SFR calculation (i.e. galaxy size, stellar mass in the bulge and disc, cold gas mass, rate of accretion on to the disc of newly cooled gas and metallicity of the cold gas) to make a consistent comparison, in which any difference will be due exclusively to the new SF law. Fig. C1 shows the ratio between the SFR calculated using a given SF law and that from the original recipe, $\rm SFR_{new}/SFR_{original}$, as a function of stellar mass (left-hand panel) and cold gas mass (right-hand panel), at $z = 0$ and 6, for the Bau05 and Bow06 models.

$\rm SFR_{new}/SFR_{original}$ versus stellar mass. At $z = 0$, the new SF laws result in larger SFR for low stellar mass central galaxies by around an order of magnitude. The exception is the KMT law in the case of the Bow06 model, which predicts a lower SFR than in the original model for low stellar mass galaxies, before rising and peaking around $M_{\rm stellar} \approx 10^{10}\,h^{-1}\,{\rm M}_\odot$. This arises from the abrupt fall in the radial $\Sigma_{\rm SFR}$ predicted by the KMT law due to the large disc sizes of low-mass galaxies in the Bow06 model (see Appendix D2). Moving to high stellar masses, in all cases the SFRs from the new laws are smaller than the original ones. In the Bau05 model, similar trends are seen for satellite galaxies. However, in the Bow06 model the predictions for satellites are quite different. This is because in the Bow06 model, satellite galaxies have, in general, more modest cold gas reservoirs compared with the Bau05 model. At $z = 6$, the predicted changes in the SFR are qualitatively similar to those seen at $z = 0$.

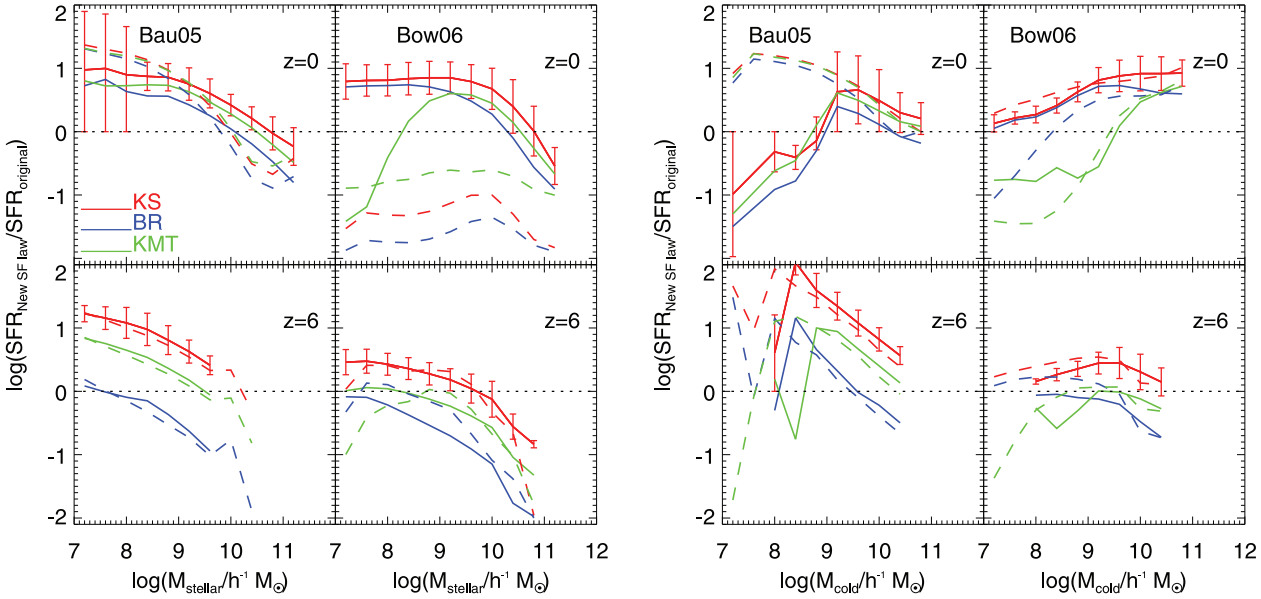

Figure C1. Ratio between the new SFR and that in the original model, $SFR_{new}/SFR_{original}$, plotted as a function of stellar mass (left-hand four panels) and of cold gas mass (right-hand four panels). The upper row shows the predictions at $z = 0$ and the lower row at $z = 6$. Within each set of four panels, the left column shows the Bau05 model and the right column shows the Bow06 model. Three representative SF laws are shown, the KS law (red), BR (blue) and KMT (green). Solid lines show the results for central galaxies only, while dashed lines show the results for satellite galaxies only. Only galaxies with $M_{cold} > 0$ are included in this plot. Error bars show the 10th and 90th percentiles of the distribution, and for clarity are shown only for the KS law.

$SFR_{new}/SFR_{original}$ versus cold gas mass. The largest differences between the new and old SF laws are observed at intermediate cold gas masses, $8 < \log(M_{cold}/h^{-1}\,M_\odot) < 10$, while the differences become generally smaller when moving to the extremes of high and low cold gas masses. This behaviour is more pronounced in the Bau05 model at all redshifts than in the Bow06 model. The non-linear dependence of the SF laws on cold gas mass is directly linked with the non-linearity of the SF time-scale with cold gas mass. Thus, we expect that changing the SF law also affects galaxies in different ways depending on their cold gas content.

APPENDIX D: OTHER OBSERVED PROPERTIES OF GALAXIES

We compare the predictions of the models with the new SF laws against selected observations.

D1 The galaxy luminosity function

The galaxy LFs in the b_J and K bands at $z = 0$ are shown in Fig. D1, for the Bau05 (top) and the Bow06 (bottom) models, and for variants with new SF laws. Perhaps surprisingly, nearly all of the new SF laws tested give a reasonably good fit to the observed LFs and follow closely the predictions of the original GALFORM models, even though we keep other parameter values fixed. Exceptions arise for the KS and the KS.thresh laws in the Bow06 model, which produce too many bright galaxies in the blue band. However, the predicted K-band LF is consistent with the observations even in these cases. This implies that the new laws result in too much SF activity at the present day in galaxies with $M_\star \geq 10^{10}\,h^{-1}\,M_\odot$ for the KS SF laws in the Bow06 model. This suggests that the AGN feedback in these objects is not strong enough, and there is still gas cooling and hence SF activity at low z. This lack of AGN feedback is a consequence of the reduced burst SF in these models at $z \leq 4$

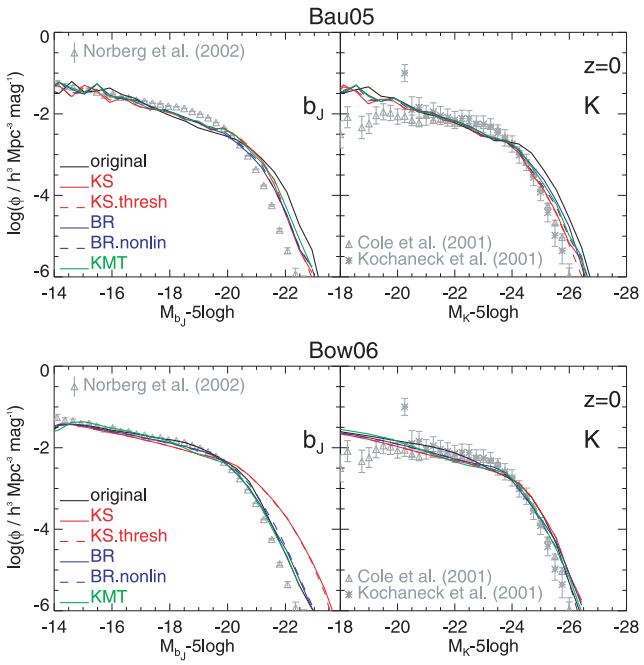

Figure D1. The b_J- (left) and K-band (right) galaxy LFs at $z = 0$. The fiducial Bau05 (top) and Bow06 (bottom) models are shown as black lines. Predictions are shown for the KS law (solid red), KS.thresh law (dashed red; K98), BR law (solid blue; BR06), BR.nonlin law (dashed blue; Dutton et al. 2010) and the KMT law (solid green; Krumholz et al. 2009b). Observational results from Norberg et al. (2002) (b_J band) and Cole et al. (2001) and Kochanek et al. (2001) (K band) are shown using grey symbols.

(see Fig. 1), which reduces the mass of the BHs formed in massive galaxies and therefore the strength of the AGN feedback (Section 2). Another indication of the absence of AGN feedback in the galaxies producing the excess in the b_J band is that they correspond to

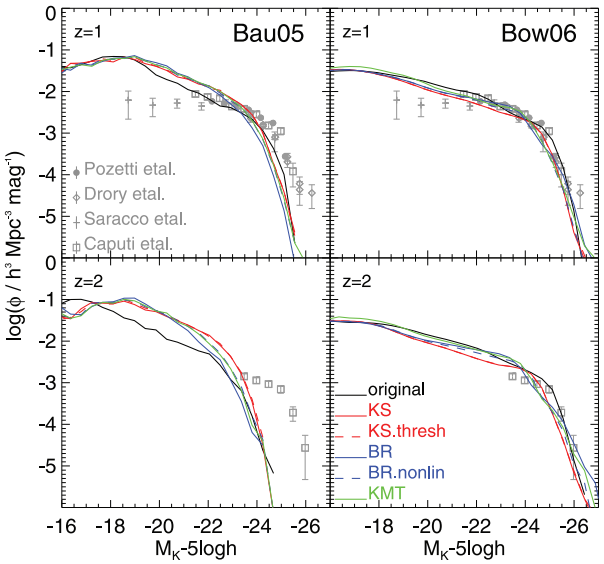

Figure D2. Rest-frame K-band galaxy LF at redshifts $z = 1$ and 2 as labelled, for the Bau05 (left) and Bow06 (right) models and the different forms of SF laws tested: KS (solid red), KS.thresh (dashed red), BR (solid blue), BR.nonlin (dashed blue) and KMT (solid green). Observational results from Pozzetti et al. (2003), Drory et al. (2004), Saracco et al. (2006) and Caputi et al. (2006) are shown as grey symbols, identified by the key in the top left-hand panel.

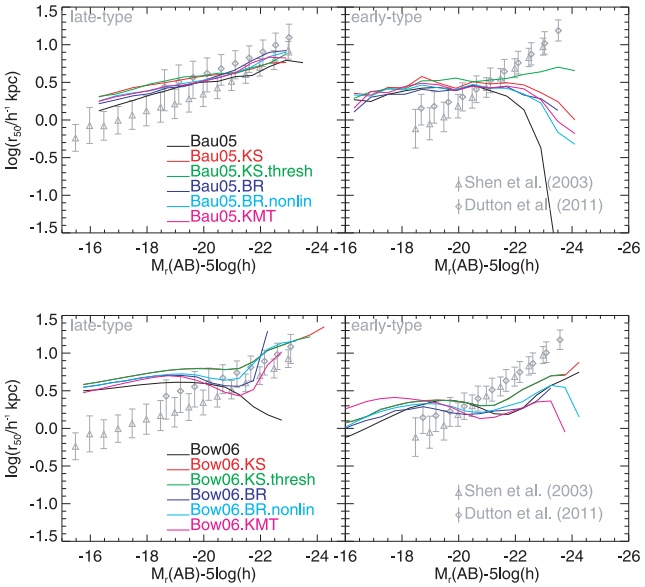

Figure D3. Galaxy half-light radius as a function of r-band magnitude for late- (top) and early-type (bottom) galaxies. Early types are defined to have a bulge-to-total luminosity ratio in the r band exceeding 0.5. Different lines and colours show the medians in the models tested as indicated by the key. The observational results from Shen et al. (2003) and Dutton et al. (2011) of late- and early-type galaxies (classified based on their Sérsic index and colours, respectively), which are both based on the SDSS, are shown as grey symbols with error bars (corresponding to the medians and 10–90 per cent of the distributions). The widths of the distributions around the median in the models are not shown for clarity, but are comparable to those of the observations (see González et al. 2009).

late-type galaxies with very low bulge-to-total stellar mass ratios (that host modest mass BHs).

The changes in the LF are particularly mild in the Bow06 model on applying the BR, BR.nonlin and KMT laws. This similarity is mainly caused by self-regulation of the SF channels (i.e. SB and quiescent SF), in which reduced quiescent SF activity at high redshift leads to galaxies characterized by massive discs and high gas fractions which experience more prominent SB activity in gas-rich mergers and disc instabilities. Thus, the overall SF remains approximately constant. This is also reflected in the mild impact on the optical colours of galaxies, e.g. $g - r$, in which the blue cloud in the colour–magnitude diagram appears slightly more pronounced when the new SF laws are applied.

At high redshifts the similarity in the predicted LFs at $z = 0$ is maintained. Fig. D2 shows the rest-frame K-band LF at $z = 1$ and 2 for the original models and variants. With the new SF laws the Bau05 model produces more galaxies at intermediate luminosities (i.e. $-16 < M_K - 5 \log\, h < -20$) at $z = 2$ compared to the original model. This arises because the bulk of the SF activity in galaxies is shifted to higher redshifts with the new SF laws (Fig. 1). Note that, even though the LF remains nearly unchanged, the contributions to the total luminosity from the bulge and disc components of galaxies are modified due to the change in the quiescent and burst SF modes. The new SF laws tend to produce twice as many ellipticals as in the original models over the whole mass range.

D2 Galaxy sizes

In GALFORM the size of a galactic disc is determined by the conservation of angular momentum of the gas cooling from the halo and the application of centrifugal equilibrium in the combined potential of the disc, bulge and host halo. Newly cooled gas modifies the angular momentum of the existing disc. Fig. D3 shows the size–luminosity relation of late- (top) and early-type (bottom) galaxies in the two models (the Bau05 model on the left and Bow06 on the right), and the variants. Early-type galaxies are defined here as those with a dust extincted bulge-to-total luminosity ratio in the r band exceeding 0.5 ($B/T > 0.5$; González et al. 2009) to approximately correspond to what is used for the SDSS samples. We also show two different observational estimates of the size–luminosity relations (Shen et al. 2003; Dutton et al. 2011), both based on SDSS data.

Considering first late-type galaxies, we find that the new SF laws produce only a small change in sizes for the Bau05 model, but a large change in the sizes of bright disc-dominated galaxies in the Bow06 model, improving the agreement with observations. At intermediate luminosities, both models agree somewhat better with the size–luminosity relation found by Dutton et al. (2011) than with that of Shen et al. (2003). The larger sizes reported by Dutton et al. are due to the 2D fitting they perform to galaxy surface brightness profiles (i.e. including separate disc and bulge components, and inclinations), in contrast with the use of circular apertures to estimate half-light radii in the case of Shen et al.

Bright spirals are larger in the Bow06 variants because the lower quiescent SFRs predicted by the new SF laws (Section 3.2) result in more massive discs compared to the original Bow06 model, which then causes more disc instabilities. (A lower SFR means less SNe feedback and consequently less cold gas ejected from the disc, hence giving a larger total mass – stars plus cold gas – for the disc.) In the original Bow06 model, bright late-type galaxies typically had quite large bulge-to-total luminosity ratios, close to the classification boundary $B/T = 0.5$, but the increased incidence of disc instabilities converts some of these to early-type galaxies. The late-type galaxies which remain have, on average, larger disc sizes than before (since smaller discs are more unstable for a given

mass). In the Bau05 model, the differences are smaller since this model already produces longer SF time-scales compared to the Bow06 model, due to the form and parameters used in the SF recipe (see Section 2.1). The failure of the Bow06 model to predict small enough sizes for faint disc-dominated galaxies might be ameliorated with a more detailed modelling of the radial distributions of stars and gas (e.g. as in Stringer & Benson 2007).

For the early-type galaxies, on the other hand, the new SF laws result in large changes in sizes for bright spheroid-dominated galaxies in the Bau05 model, but only modest changes in the Bow06 model. The sizes of spheroids are driven by their formation through mergers and disc instabilities. The flatness of the predicted size–luminosity relations for spheroid-dominated galaxies in comparison with observations may result from the simplified calculation of the sizes of merger remnants, rather than implying that an additional mechanism is needed (see Almeida et al. 2007; González et al. 2009).

This paper has been typeset from a TEX/LATEX file prepared by the author.